Bacillus thuringiensis Cry1A toxins divert progenitor cells toward enteroendocrine fate by decreasing cell adhesion with intestinal stem cells

Rouba Jneid[1,2,*], Rihab Loudhaief[1], Nathalie Zucchini-Pascal[1], Marie-Paule Nawrot-Esposito[1], Arnaud Fichant[1,3], Raphaël Rousset[1], Mathilde Bonis[3], Dani Osman[2] and Armel Gallet[1]

[1] Université Côte d'Azur, CNRS, INRAE, ISA, France
[2] Faculty of Sciences III and Azm Center for Research in Biotechnology and its Applications, LBA3B, EDST, Lebanese University, Tripoli, Lebanon
[3] Laboratory for Food Safety, University Paris-Est, French Agency for Food, Environmental and Occupational Health & Safety (ANSES), 94700 Maisons-Alfort, France.
Corresponding author: A. Gallet, ISA, UMR CNRS 7254/INRAE 1355/UCA, 400 route des Chappes, BP 167, 06903 Sophia Antipolis Cedex, France. gallet@unice.fr
*Present address: Department of Biology, Faculty of Science, University of Copenhagen, Copenhagen O, Denmark

Abstract

Bacillus thuringiensis subsp. *kurstaki* (*Btk*) is a strong pathogen toward lepidopteran larvae thanks to specific Cry toxins causing leaky gut phenotypes. Hence, *Btk* and its toxins are used worldwide as microbial insecticide and in genetically modified crops, respectively, to fight crop pests. However, *Btk* belongs to the *B. cereus* group, some strains of which are well known human opportunistic pathogens. Therefore, ingestion of *Btk* along with food may threaten organisms not susceptible to *Btk* infection. Here we show that Cry1A toxins induce enterocyte death and intestinal stem cell (ISC) proliferation in the midgut of *Drosophila melanogaster*, an organism non-susceptible to *Btk*. Surprisingly, a high proportion of the ISC daughter cells differentiate into enteroendocrine cells instead of their initial enterocyte destiny. We show that Cry1A toxins weaken the Cadherin-dependent adherens junction between the ISC and its immediate daughter progenitor, leading the latter to adopt an enteroendocrine fate. Hence, though not lethal to non-susceptible organisms, Cry toxins can interfere with conserved cell adhesion mechanisms, thereby disrupting intestinal homeostasis and enteroendocrine functions.

Keywords

Cry1A toxins, *Bacillus thuringiensis*, *Drosophila melanogaster*, Intestinal Stem cells, enteroendocrine cells, Cadherins

Introduction

The gut lining is undergoing constant damage caused by environmental aggressors (pesticides, drugs, viruses, bacteria and toxins) ingested along with food. The gut quickly responds to these aggressions by accelerating its epithelium renewal to replace damaged cells. Over the past decade, studies in *Drosophila melanogaster* have contributed substantially to the understanding of the cellular and molecular mechanisms controlling the maintenance of intestinal homeostasis and regeneration. These mechanisms have proven to be highly conserved in the animal kingdom. In *Drosophila*, resident intestinal stem cells (ISCs) are the guarantors of this cell renewal process. Under normal conditions, asymmetric division of an ISC gives rise to a new ISC (to maintain the pool of ISC) and to a daughter progenitor cell that can commit to two different paths of differentiation. The enteroblasts (EBs) and enteroendocrine precursors (EEPs) are the precursors of enterocytes (ECs) and enteroendocrine cells (EECs), respectively (Guo et al., 2021; Joly and Rousset, 2020; Pasco et al., 2015). ECs are the main intestinal epithelial bricks constituting an efficient barrier against aggressors and are therefore their first victims. The damaged or dying ECs emit cytokines, which stimulate the proliferation of ISCs to augment the pool of EBs that will differentiate into ECs to replace the damaged ones (Bonfini et al., 2016; Osman et al., 2012). Two mechanisms underlying intestinal regeneration have been described. The first one is the "cell renewal" model, which occurs under weak aggression conditions that does not induce EC apoptosis. In this case, ISC proliferation is low and the neo-EBs differentiate into ECs. However, this provokes a transient excess of ECs due to the absence of prior EC death. The gut cell homeostasis is subsequently reestablished by the removal of old ECs (Loudhaief et al., 2017). The second mechanism, called "cell replenishment" or "regenerative cell death", occurs after a strong aggression that induces massive EC apoptosis. In this case, a rapid ISC proliferation is followed by the differentiation of EBs into ECs to replace the dying ones (Loudhaief et al., 2017; Vriz et al., 2014) without producing supernumerary ECs.

Bacillus thuringiensis (*Bt*) bacteria are largely used as microbial insecticides to fight crop pests. *Bt* is a Gram-positive sporulating bacterium belonging to the *Bacillus cereus* (*Bc*) group (Ehling-Schulz et al., 2019). It was first identified and characterized for its specific entomopathogenic properties due to the presence of a crystal containing specific Cry protoxins, which are produced during the bacteria sporulation (Rabinovitch et al., 2017). Among all the subspecies of *Bt* inventoried (http://www.bgsc.org/), spores of *Bt* subsp. *Kurstaki* (*Btk*) are used to

2

67   specifically kill lepidopteran larvae that threaten crops, through a cocktail of Cry toxins made of

68   Cry1Aa, Cry1Ab, Cry1Ac, Cry2Aa and Cry2Ab (Caballero et al., 2020). Cry toxins sequentially

69   bind to different receptors present in the midgut to exert their cytotoxicity. Among those receptors,

70   the ones named Bt-R that belong to the Cadherin transmembrane cell adhesion molecules are

71   primordial for the Cry1A holotype of toxins, allowing them to bind to enterocyte brush borders.

72   The other receptors—such as Alkaline phosphatases, Aminopeptidases N, and ABC transporters—

73   appear to account for the cytotoxicity that Cry exert toward susceptible organisms (Adang et al.,

74   2014; Gao et al., 2019; Li et al., 2020; Liu et al., 2018b). In susceptible insects, upon ingestion of

75   spores and crystals, the basic midgut pH dissolves the crystals, releasing the Cry protoxins. Then,

76   digestive enzymes cleave Cry protoxins (130kD and 72kD for proCry1A and proCry2A,

77   respectively) into activated Cry toxins (around 67kD) allowing them to bind their midgut

78   receptors. Thereby, Cry toxins form pores in the plasma membrane of ECs, ultimately leading to

79   their death. An alternative mode of action of Cry toxins suggested that Cry binding to Cadherin

80   induces an intracellular flux of Mg^{2+} resulting in EC apoptosis (Castella et al., 2019; Mendoza-

81   Almanza et al., 2020). In both models, toxin-induced breaches within the gut lining allow bacteria

82   (spores and vegetative cells) to reach the internal body cavity, generating a septicemia and

83   subsequent death of the lepidopteran larvae within 2 or 3 days after ingestion of *Btk* spores

84   (Mendoza-Almanza et al., 2020). It is assumed that *Btk* do not harm the intestine of non-susceptible

85   organisms because, first, the intestinal pH is not suitable for the solubilization of the crystal of

86   protoxins and, second, the Cry toxin receptors are absent from their gut epithelium (Rubio-Infante

87   and Moreno-Fierros, 2016).

88   However, recent studies provide evidence that *Btk* also exhibits some adverse effects on

89   non-susceptible organisms including humans. Indeed, strains of the *B. cereus* group, to which *Bt*

90   belongs, are well-known worldwide food-poisoning pathogens causing diarrheal-type illnesses due

91   to the production of enterotoxins during the vegetative phase in the intestine (Ehling-Schulz et al.,

92   2019; Glasset et al., 2016; Jovanovic et al., 2021). Recently, *Bt* has also been implicated in

93   foodborne outbreak events and the strains identified were indistinguishable from the commercial

94   ones (Biggel et al., 2021; Bonis et al., 2021; Johler et al., 2018). Furthermore, we have shown that

95   *Btk* spores and toxins at concentrations close to those recovered on vegetables after spraying induce

96   growth defects and developmental delay in *Drosophila* larvae (Nawrot-Esposito et al., 2020).

97   Increasing spore and toxin doses ultimately led to larval lethality (Babin et al., 2020). Cry toxins

98   produced by *Btk* are also used in genetically modified crops (GMCs) (ISAAA, 2017), and it has

99   been reported that GMC-produced Cry1Ab toxin is found in agricultural water stream networks at

100 abnormally high doses that may affect the survival rate of non-susceptible insects (Rosi-Marshall

101 et al., 2007). In a similar vein, laboratory studies have demonstrated genotoxic activity of Cry1Aa,

102 Cry1Ab, Cry1Ac and Cry2A in zebrafish rearing water (Grisolia et al., 2009). Based on all these

103 data, our aim in this study was to decipher the interaction of *Btk* and its toxins with the intestinal

104 epithelium using *Drosophila melanogaster*, an organism non-susceptible to *Btk* Cry toxin and a

105 well-established model for studying host-pathogen interaction mechanisms.

106   Using environmental doses of spores and crystals of protoxins recovered on vegetables

107 after treatment, we first showed that crystals of *Btk* Cry protoxins induced moderate enterocyte

108 death that triggers a quick cell replenishment by favoring symmetric ISC divisions. We then

109 demonstrated that the crystals diverted a higher number of progenitor cells from their initial EC

110 fate toward an EEC fate, generating an excess of EECs. Importantly, this effect was due to a

111 weakened cell-cell interaction between ISC mother cells and progenitor daughter cells. We were

112 able to rescue the Crystal-dependent excess of EECs by specifically overexpressing the DE-

113 Cadherin in ISC and progenitor daughters, reinforcing the strength of the adherens junction

114 between these cells. Moreover, we found that among the five *Btk* Cry toxins, only the Cry1A

115 holotype was able to induce this EEC excess. Unexpectedly, we observed that *Btk* crystals are

116 processed in the midgut of adult *Drosophila* as they are in that of susceptible-organisms, releasing

117 activated Cry1A toxins. Hence, since our data demonstrate that Cry1A toxins disrupt conserved

118 cellular processes, many non-susceptible organisms may exhibit an excess of EECs and

119 consequently a disruption of their enteroendocrine functions.

120

Results

Crystals of *Btk* Cry protoxins induce EC death and stimulate proliferation of intestinal stem cells

124 During sporulation*, Btk* produces a crystal of protoxins that is lethal to lepidopteran larvae once

125 ingested by the insect. To study the *Btk* effects on the non-susceptible organism *Drosophila*

126 *melanogaster*, we orally infected flies with the SA11 *Btk* strain (hereafter named *Btk^{SA11}*), which

127 is widely utilized in commercial microbial insecticides. A suspension of spores/crystals in water

128   was deposited on the fly medium corresponding to 10^6 CFU (Colony Forming Unit) of spores per

129   female for 4 cm². The impact on the gut of the spores alone, or the toxins alone, was also monitored

130   using a *Btk* strain devoid of protoxin crystals ($Btk^{\Delta Cry}$) or purified crystals, respectively (see

131   Materials and Methods).

132   The *Gal4/UAS* binary expression control system (Brand and Perrimon, 1993) allowed us

133   to monitor first the effect of the spores/crystals on EC apoptosis by expressing the Caspase 3

134   sensor (Casp::GFP; (Schott et al., 2017) under the control of the *myo1A-Gal4* EC driver

135   (*myo1A>Casp::GFP*). With this transgenic combination, the GFP is detectable only when the

136   Caspase 3 is activated in ECs. As a negative control, we fed flies with water alone. In all our

137   experiments, we focused our observations on the posterior midgut (R4 region,

138   https://flygut.epfl.ch/overview) (Buchon et al., 2013) because this region is known to show a high

139   stem cell renewal activity (Marianes and Spradling, 2013) and exhibits the strongest phenotypes

140   (see below). One day post-ingestion, Btk^{SA11} or purified crystals induced moderate apoptosis of the

141   ECs compared to the control (Figure 1A). However, the treatment with spores alone devoid of

142   protoxin crystals ($Btk^{\Delta Cry}$) did not induce EC death.

143   Induction of cell death is known to strongly induce ISC proliferation in the whole midgut

144   (Biteau et al., 2008; Chatterjee and Ip, 2009; Jiang et al., 2009; Loudhaief et al., 2017). This

145   prompted us to assess the number of ISC mitoses in the different conditions, using an Anti-

146   phospho-Histone H3 antibody marking mitotic cells. As expected, ISC mitotic indexes were

147   stronger upon oral infection with Btk^{SA11} spores or purified crystals than in the control (Figure 1B).

148   In $Btk^{\Delta Cry}$ spore infection, mitotic figures were only moderately increased (Figure 1B). This is

149   consistent with previous observations showing that a low dose (10^6 CFU per *Drosophila*) of *Btk*

150   vegetative cells (that do not produce and contain crystals of Cry protoxins) only moderately

151   activates ISC proliferation without inducing EC apoptosis (Loudhaief et al., 2017). We confirmed

152   this increase in ISC proliferation by counting the total number of ISCs in the posterior midgut (R4

153   region). To specifically mark ISCs, we expressed the GFP under the control of the *Dl-Gal4* driver

154   that is expressed in ISCs and EEPs (Joly and Rousset, 2020), and we co-stained with an anti-

155   Prospero (Pros), an EEP and EEC marker (ISCs were therefore GFP+, Pros-). While we observed

156   an increase in ISC number with Btk^{SA11} spores or purified crystals, $Btk^{\Delta Cry}$ spores did not induce

157   any increase (Figure 1C). This could be explained by the fact that the moderate stimulation of ISC

158   proliferation by $Btk^{\Delta Cry}$ spores was not sufficient to promote a detectable increase in global ISC

159 number. Another possibility could be that $Btk^{\Delta Cry}$ spores favor asymmetric ISC division, giving

160 rise to one ISC and one precursor (EB or EEP), while Btk^{SA11} spores or purified crystals promoted

161 symmetric ISC division, giving rise to two ISCs. Indeed, numerous observations show that in the

162 *Drosophila* midgut during intestinal homeostasis, the main mode of ISC division is asymmetric,

163 accounting for about 70-80% of the mitosis. On the contrary, following an urgent need such as

164 detrimental bacterial infection, ISCs divide symmetrically to allow faster regeneration of the tissue

165 (de Navascues et al., 2012; Goulas et al., 2012; Joly and Rousset, 2020; O'Brien et al., 2011; Tian

166 and Jiang, 2014; Zhai et al., 2017). To assess the mode of ISC division, we used the ReDDM

167 *Drosophila* genetic tool (Antonello et al., 2015) under the control of the *Dl-Gal4* driver (*Dl-*

168 ReDDM). This tool allows us to follow the progeny of the ISCs because they express a stable RFP

169 (H2B::RFP) while the mother cells (the ISCs) express a labile GFP that disappears in less than 24

170 hours. After shifting the flies to 29°C to activate the *Dl*-ReDDM tool, the GFP was only expressed

171 in Dl+ cells (i.e. the ISCs and EEPs) while the H2B::RFP was expressed in Dl+ cells but also

172 stably transmitted to the progeny. When two cells in direct contact were ISC/ISC

173 (GFP+/H2B::RFP+) or EEP/EEP (GFP+/H2B::RFP+/Pros+) or EB/EB (only RFP+), we

174 considered they were coming from a symmetric division. In contrast, divisions were considered

175 asymmetric when two neighboring cells displayed a different combination of immunolabelling,

176 revealing that their identities were different. Interestingly while we observed a 33%/67%

177 distribution of symmetric/asymmetric division in the control conditions (Figure S1A and S1B),

178 the mode of division trended in favor of symmetric with $Btk^{\Delta Cry}$ spores (58.6%/41.4%) and was

179 completely reversed with the Btk^{SA11} spores (74.2%/25.8%) (Figure S1A and S1B). Therefore,

180 consistent with previous studies, the mode of ISC division appeared to reflect the degree of

181 intestinal damage, the symmetric mode being preferentiality adopted when the damage was greater

182 (i.e., when cell death occurred).

183 We next monitored the number of ECs using the fly strain *myo1A>GFP* allowing the

184 expression of GFP in all ECs. $Btk^{\Delta Cry}$ spores induced an excess of ECs at days 1 and 3 post-

185 ingestion; the right number of ECs was recovered 5 days after ingestion (Figure 1D and Figure

186 S1C). Along with the absence of EC apoptosis (Figure 1A) and the moderate induction of ISC

187 proliferation (Figure 1B), our data strongly suggest that $Btk^{\Delta Cry}$ spores weakly damage the

188 intestinal epithelium, reminiscent of the "cell renewal" process previously described after infection

189 with poorly virulent bacteria (Loudhaief et al., 2017). On the contrary, ingestion of the Btk^{SA11}

6

190   spores or purified crystals provoked a decrease in EC number 3 days post-ingestion (Figure 1D

191   and Figure S1C) that we attributed to EC apoptosis (Figure 1A) (Loudhaief et al., 2017). A normal

192   number of ECs was restored 5 days post-ingestion for Btk^{SA11} spores and to a lesser extent for

193   purified crystals (Figure 1D and Figure S1C). Hence, Btk^{SA11} spores or purified crystals launch a

194   process of regenerative cell death, inducing a strong proliferation of ISCs to quickly replenish the

195   gut lining as previously described for strong pathogens (Vriz et al., 2014). Importantly, the

196   ingestion of purified crystals containing the Btk Cry-protoxins recapitulates the midgut phenotypes

197   caused by the ingestion of Btk^{SA11} spores.

Btk^{SA11} spores induced an increase in EB, EEP and EEC numbers

199   During the course of our experiments we observed that many more EECs were apparently present

200   in the flies that had ingested Btk^{SA11} spores compared with in the control flies (Figure S2A and

201   S2C). As ECs derive from EBs and EECs from EEPs, we assessed the amount and the identity of

202   the precursors in the different conditions of infection (H₂O; $Btk^{\Delta Cry}$ spores, Btk^{SA11} spores and

203   purified crystals). To count the EBs, we used a $Gal4$ strain of $Drosophila$ driving GFP expression

204   specifically in EBs ($Su(H)>CD8::GFP$). As expected, a significant increase in the number of EBs

205   was observed between the first and the fifth day after ingestion of $Btk^{\Delta Cry}$, Btk^{SA11} or purified

206   crystals (Figure 2A). The EEP number was assessed using two markers: the GFP expressed in

207   ISCs and progenitors (EBs and EEPs) using the $esg-Gal4$ driver ($esg>GFP$) and a Pros staining

208   which labels EEPs and EECs. Cells expressing both GFP and Pros corresponded to EEPs. While

209   $Btk^{\Delta Cry}$ spores did not modify the number of EEPs, ingestion of either Btk^{SA11} spores or purified

210   crystals resulted in an increase in EEPs from day one onwards (Figure 2B and D). Since EEPs

211   must differentiate into EECs, we then counted the differentiated EECs that were GFP- Pros+. No

212   difference in EEC number was obtained with $Btk^{\Delta Cry}$ spores compared to the control, whereas there

213   was a net increase with the Btk^{SA11} spores and with the purified crystals (Figure 2C, D and S2A-

214   D). Interestingly, though this event was rare, we also observed that EEPs could undergo a cycle of

215   mitosis that might contribute to the increase in EEPs and EECs (Figure 2E) (Biteau and Jasper,

216   2014; Li et al., 2014; Zeng and Hou, 2015). Interestingly, we never observed such an increase in

217   EEPs and EECs in the anterior part of the midgut (Figure S2E-I). Altogether, our results showed

218   that the protoxin crystals of Btk^{SA11} were responsible for the excess of EECs in the posterior midgut.

EEC excess arises from newborn EEPs after ingestion of crystals of Btk^{SA11} protoxins

7

220   To demonstrate that the excess of EEPs and EECs arose from proliferating ISCs caused by the

221   ingestion of protoxin crystals, we used the ReDDM cell lineage tracing system using the *esg-Gal4*

222   driver (*esg-ReDDM* flies). We chose to analyze the progeny at day 3 post-ingestion (Figure 3A),

223   when the increase in EECs reached its peak (Figure 2C). According to the expression of specific

224   cell markers and nucleus size, we could identify different cell types either that existed before the

225   ingestion or that appeared after the ingestion of $Btk^{\Delta Cry}$ spores, Btk^{SA11} spores or purified crystals.

226   Identities of the different cell types were defined as follows: ISCs were GFP+ RFP+ DAPI+ with

227   small nuclei; EBs were GFP+ RFP+ DAPI+ with bigger nuclei; EEPs were GFP+ RFP+ Pros+

228   DAPI+; new EECs were RFP+, Pros+ DAPI+; old EECs were Pros+ DAPI+, new ECs were RFP+

229   DAPI+ with big polyploid nuclei and old ECs were DAPI+ with very big nuclei (Figure 3 B-E").

230   In the control experiments, a few newborn ECs (red arrows in Figure 3B and B', and Figure 3G)

231   and rare newborn EECs (Figure 3F) appeared 3 days post-ingestion, reflecting the relative steady

232   state of the cellular homeostasis. As expected for poorly virulent bacteria, ingestion of $Btk^{\Delta Cry}$

233   spores induced the appearance of newborn ECs (red arrows in Figure 3C, C' and Figure 3G) and

234   only rare newborn EECs resulted (pink arrows in Figure 3C-C" and Figure 3E and G). Similarly,

235   ingestion of Btk^{SA11} spores or purified crystals promoted the appearance of newborn ECs (red

236   arrows in Figure 3D, D', E and E' and Figure 3G) but, strikingly, a high number of newborn EECs

237   appeared (pink arrows in Figure 3D-E" and F). However, we could not rule out the possibility that

238   the Btk^{SA11} spores altered EB behavior, pushing them toward an EEC fate. To verify this possibility,

239   we carried out a ReDMM lineage tracing using the *Su(H)-Gal 4* driver that is specifically expressed

240   in EBs (*Su(H)-ReDDM* flies). In this case, no newborn EECs were detectable upon ingestion of

241   the Btk^{SA11} spores while many newborn ECs were present (Figure S3A-C), indicating that EBs are

242   not the source of the increase in the number of EECs.

243   Altogether, our data demonstrate that ingestion of Btk^{SA11} spores damages the intestinal

244   epithelium, strongly stimulating symmetric ISC proliferation. However, some of the progenitors

245   make the choice to commit to an EEP/EEC fate instead of an EB/EC fate. Consequently, there is

246   a lack of new ECs to replace the dying ones and there is an excess of EECs. Interestingly, the

247   crystals containing the Cry protoxins can recapitulate all the Btk^{SA11} spore effects. In contrast, the

248   effect of $Btk^{\Delta Cry}$ spores is less damaging for the gut epithelium. In this case, ISC proliferation is

249   only weakly stimulated and the progenitors make the choice to commit to the EB/EC fate to replace

250   the damaged ones.

Crystals of *Btk^{SA11}* protoxins decrease ISC-Progenitor cell-cell adhesion

It is well established that the Notch (N) signaling pathway governs progenitor differentiation and cell lineage choice in the adult *Drosophila* midgut (Micchelli and Perrimon, 2006; Ohlstein and Spradling, 2006; Ohlstein and Spradling, 2007; Pasco et al., 2015). Indeed, the transmembrane ligand Delta (Dl) expressed in ISCs binds to its N receptor present on the surface of progenitors. This induces the cleavage of the intracellular domain of N and its relocation into the nucleus to activate its target genes (Perdigoto and Bardin, 2013). Upon N activation, progenitors differentiate into EBs and then into ECs while in the absence/weak activation of N signaling, progenitors commit to an EEP/EEC fate (Beehler-Evans and Micchelli, 2015; Guo and Ohlstein, 2015; Ohlstein and Spradling, 2007; Sallé et al., 2017). A prolonged and/or strong interaction between the ISC and its progenitor is necessary to reach the threshold of the N signaling activation sufficient to commit the progenitor to the EB/EC fate. A shorter and/or weaker interaction between the ISC and its progenitor weakly induces the N pathway, pushing the progenitor towards the EEC fate (Guisoni et al., 2017; Sallé et al., 2017). The adherens junctions between ISCs and progenitors formed by E-Cadherins and Connectins intervene to prolong the contact between Dl and N, favoring the EB/EC fate (Choi et al., 2011; Falo-Sanjuan and Bray, 2021; Maeda et al., 2008; Zhai et al., 2017). As the consensus receptors for Cry1A toxins in target organisms are members of the Cadherin family (Adang et al., 2014), we wondered whether the *Btk^{SA11}* could interfere with the function of the adherens junctions. We hypothesized that ISC-progenitor interaction could be reduced via interference of Cry toxins with Cadherins, modifying the progenitor cell fate and thus explaining the excess in EEC number seen after ingestion of *Btk^{SA11}* spores or purified crystals. To test this hypothesis, we labelled the intestines of *esg>GFP Drosophila* fed with *Btk^{ΔCry}* spores, *Btk^{SA11}* spores or purified crystals with the anti-Armadillo (Arm)/β-catenin antibody that strongly marks the adherens junctions. We observed an intense labeling at the level of the ISC-progenitor junctions in the control (Figure 4A-A' and I) or following intoxication by *Btk^{ΔCry}* spores (Figure 4C-C' and I). Strikingly, this labeling became less intense following ingestion of *Btk^{SA11}* spores or purified crystals (Figure 4E-E', G-G' and I). We confirmed these observations using a *Drosophila* line expressing the endogenous DE-Cadherin (DE-Cad) fused to a Tomato tag (Figure 4 B, D, F and H). Moreover, we observed that the decrease in Tomato::DE-Cad labelling between an ISC and its progenitor was correlated with the expression of EEP markers (blue stars in figure 4B and F and H). Our results suggested that crystals of Cry protoxins produced by *Btk^{SA11}* are responsible

282   for the increase in the number of EEPs/EECs, this effect being associated with a decrease in

283   intercellular adhesion between ISCs and progenitors.

284   **Increasing adherens junction strength rescues crystal-dependent cell fate diversion.**

285   To confirm that the crystals of Btk^{SA11} interfered with progenitor fate by disturbing adherens

286   junctions, we wondered whether increasing the strength of cell adhesion between ISCs and

287   progenitors could rescue the right number of EEPs/EECs. Thus, we overexpressed the DE-

288   Cadherin in these cells using the *esg-ReDDM* flies (Figure 5 and S4A-D'). We analyzed the identity

289   of newborn cells 3 days after ingestion of water (control), $Btk^{ΔCry}$ or Btk^{SA11} spores, or purified

290   crystals. Interestingly, in flies overexpressing the DE-Cadherin in ISCs and progenitors fed with

291   Btk^{SA11} spores or purified crystals, we no longer observed an increase in the number of EECs (blue

292   arrows in Figure 5A-D, and Figure 5E). In agreement, the number of ISC-progenitor pairs with a

293   strong interaction was increased (Figure 5F compared to Figure 4I). Furthermore, as expected,

294   newborn ECs appeared (red arrows in Figure 5B-D'), strongly suggesting that increasing the cell

295   adhesion between ISCs and progenitors rescued the progenitor fate disturbance generated by the

296   Btk^{SA11} crystals. Surprisingly, overexpressing the Connectin, another cell adhesion molecule,

297   which mediates hemophilic cell-cell adhesion (Zhai et al., 2017), in both ISCs and progenitors did

298   not rescue the number of EECs following feeding with Btk^{SA11} spores or purified crystals (Figure

299   S5). To confirm the disturbance of DE-Cadherin-dependent cell adhesion by purified crystals, we

300   carried out an aggregation assay in *Drosophila* S2 cell culture. Indeed, S2 cells do not

301   endogenously express the DE-Cadherin and display only a weak cell-cell adhesion phenotype

302   (Toret et al., 2014). Transfection of S2 cells with a plasmid encoding a DE-Cadherin::GFP fusion

303   resulted in large aggregate formation as early as 1h post-agitation (Ctrl in Figure 5G and S4E).

304   Adding purified crystals to the cell culture medium strongly reduced the size of aggregates.

305   Interestingly, purified Cry1Ab and Cry1Ac protoxins have the same effect although Cry1Ab

306   needed a longer time to reduce the size of S2 cell aggregates (Figure 5G-G" and S4E). Because

307   Cadherins serve as receptors for the Cry1A toxin family in target Lepidoptera (Adang et al., 2014),

308   our data suggest that in non-target organisms such as *Drosophila melanogaster*, Cry1A toxins

309   could interfere physically with the well-conserved E-Cadherin.

310   **Cry1A toxins mimic Btk^{SA11} spore effects**

10

311   *Btk*^SA11^ produces 5 different Cry toxins (Cry1Aa, Cry1Ab, Cry1Ac, Cry2Aa, and Cry2Ab)

312   (Caballero et al., 2020). We investigated whether the increase in EEP/EEC number was due to all

313   toxins present in the crystals or to only one family of toxins (i.e., the Cry1A or Cry2A family). We

314   made use of the *Btk*^Cry1Ac^ strain (referred to as 4D4 in http://www.bgsc.org/) which produces

315   crystals composed only of the Cry1Ac protoxin. We fed *esg>GFP* flies either with spores of

316   *Btk*^Cry1Ac^ or with purified Cry1Ac crystals. In both conditions, we observed a significant increase

317   in the number of EEPs and EECs 3 days post-ingestion compared to controls (Figure 6A and S6A,

318   C and D). To verify whether other toxins of the Cry1A family induced a similar rise in EEP/EEC

319   number, we generated a *Btk*^Cry1Ab^ strain (see Material and Methods) producing only the Cry1Ab

320   toxins (Figure S6I). Similar to the *Btk*^Cry1Ac^ spores, *Btk*^Cry1Ab^ spores induced an increase in

321   EEP/EEC numbers (Figure 6B and S6B). Unfortunately, no *Btk* strain yielding only Cry2A-

322   containing crystals was available and we were unsuccessful in generating one. To overcome this,

323   we used heterologous expression of Cry toxins in *E coli.* We first checked whether Cry1Ac

324   protoxin produced and purified from *Escherichia coli* (*E. coli*) was indeed able to induce an

325   increase in EEP/EEC numbers. We also forced the activation of the Cry1Ac protoxin into an

326   activated form *in vitro* (see Material and Methods). Interestingly, both the protoxin and the

327   activated form of Cry1Ac were able to induce the expected phenotype, though the activated

328   Cry1Ac form was more efficient (Figure 6C and Figure S6E and F). Conversely, both Cry2Aa

329   protoxin and its activated form purified from *E coli* were unable to increase the number of

330   EEP/EECs (Figure 6C and Figure S6G and H). Therefore, our data demonstrate that ingestion of

331   Cry1A toxins was sufficient to induce a rise in the numbers of both EEPs and EECs.

332   **Cry1A Protoxins from *Btk* crystals are activated in the *Drosophila* midgut**

333   Our data above showed that purified activated Cry1Ac toxin was more efficient for inducing an

334   EEP/EEC excess than the purified Cry1Ac protoxin. Interestingly, the magnitude of EEP/EEC

335   excess was similar using either Cry1Ac crystals or purified activated Cry1Ac toxin (compare

336   Figure 6A and 6C), suggesting that Cry1Ac protoxins contained in the crystals were activated in

337   the *Drosophila* intestine. However, the admitted model proposes that protoxins can be activated *in*

338   *vivo* only in the intestine of the susceptible lepidopteran owing to the presence of appropriate

339   digestive proteases specifically functioning at the basic pH and reducing conditions encountered

340   in the larval midgut of lepidopteran (Pardo-Lopez et al., 2012; Soberon et al., 2009; Vachon et al.,

341   2012). We therefore wondered whether the effects we observed *in vivo* were due to the crystal on

342   its own (i.e., protoxins) or to the activated Cry toxins after processing in the *Drosophila* midgut.

343   We first monitored by Western Blot the processing of the Cry1A toxin family in the fly midgut

344   fed with *Btk^SA11* spores. We used an anti-Cry1A antibody raised against the activated form of the

345   toxin, which therefore recognizes both forms (Babin et al., 2020). As a control, we incubated

346   *Btk^SA11* spores *in vitro* in water, at 25°C for 4h, 1d, 3d and 6d. Under these conditions, the protoxin

347   form of Cry1A at 130kD was predominant and stable for at least 3 days before fading (control in

348   Figure 6D, right part of the blot). This observation is in agreement with the fact that the half-life

349   of Cry1A crystals has been estimated at about 1 week in soil or under laboratory conditions at

350   25°C (Hung et al., 2016). We used the same initial *Btk^SA11* spore preparation (0h) to feed the flies.

351   We further dissected intestines and extracted total proteins at different times post-feeding.

352   Interestingly, as early as 4h, we observed the 67kD activated form of the Cry1A toxins (Figure 6D

353   left part). Noteworthy, the 130kD protoxin forms were still present, as the flies kept ingesting

354   spores and crystals throughout the experiments. Six days after ingestion, almost no more protoxins

355   or toxins were detectable due to the instability of the crystals (Figure 6D). Thus, our data show

356   that the crystals can be processed in the midgut of adult *Drosophila* to give rise to active forms of

357   the Cry1A toxins.

358   As mentioned previously, the increase in EEPs/EECs numbers was prominent in the

359   posterior midgut (Figure S2). We therefore wondered whether Cry1A crystals were differentially

360   processed along the midgut. We fed flies with purified *Btk^SA11* crystals and 24h later, we dissected

361   and crushed the intestines by separating the anterior midgut from the posterior part. Furthermore,

362   we performed subcellular fractioning by separating the soluble fraction (considered as the cytosol-

363   enriched fraction) and the insoluble fraction containing membranes. Interestingly, we observed

364   that protoxins were already activated in the anterior part of the midgut (the 67kD form) but were

365   only associated with membranes (Figure 6E). In the posterior midgut, we detected a stronger

366   quantity of the 67kD-activated form both at the membrane and in the cytosol, suggesting an

367   internalization by epithelial cells (Figure 6E). In this part of the midgut, smaller forms appeared

368   mainly associated with the membrane, probably resulting from degradation processes. Notably,

369   we did not detect the 130kD protoxins in the cytoplasmic fraction of both anterior and posterior

370   midguts, suggesting that the protoxins remained associated with membranes. Moreover, total

371   processing was never achieved since some protoxins still remained detectable. Altogether, our data

372   show that crystals containing Cry1A protoxins are processed all along the adult *Drosophila* midgut

373   to generate activated Cry1A toxins.

374

Discussion

376   Our results show that the Cry1A toxin family of *Btk* disrupts the gut cellular homeostasis of the

377   non-susceptible organism *Drosophila melanogaster*. Cry1A induces EC death coupled to an

378   increase in ISC proliferation to replace the damaged ECs. Importantly, Cry1A toxins also altered

379   intestinal cell composition by weakening DE-Cadherin-dependant cell-cell adhesion which is

380   normally highly enriched in adherens junctions linking ISCs to their immediate progenitors (Choi

381   et al., 2011; Maeda et al., 2008; Ohlstein and Spradling, 2006; Zhai et al., 2017). As a consequence,

382   progenitors are pushed toward the EEC path of differentiation instead of the EC, owing to reduced

383   activation of N signaling in progenitors (Figure 7) (Guo and Ohlstein, 2015; Maeda et al., 2008;

384   Ohlstein and Spradling, 2006; Ohlstein and Spradling, 2007; Pasco et al., 2015; Zhai et al., 2017).

385   Our data confirmed that the duration and/or the strength of the cell-cell contact between the ISC

386   and its progenitor daughter cell is important to drive the progeny toward an appropriate fate.

387   Indeed, it has been shown both in *Drosophila* and in mammalian cell culture that adherens

388   junctions are crucial to reinforce the contact between neighboring cells to allow the activation of

389   N signaling (Falo-Sanjuan and Bray, 2021; Shaya et al., 2017; Zhai et al., 2017), N being necessary

390   for the EB-EC cell fate choice.

391   Only the Cry1A family of toxins induces an increased number of EECs while Cry2A toxins

392   do not display any phenotype. Previous studies showed that Cry1A and Cry2A bind to different

393   receptors in the intestinal epithelium of susceptible lepidopteran larvae, and proteins of the

394   Cadherin family appear essential for Cry1A, but not Cry2A, binding (Adang et al., 2014; Gao et

395   al., 2019; Hernández-Rodríguez et al., 2013; Li et al., 2020; Liu et al., 2018a). *Drosophila*

396   possesses 17 genes encoding for members of the Cadherin superfamily (Hill et al., 2001). Cad88C

397   is the most similar to Bt-R Cadherin of susceptible lepidoptera, but shares only 17% of identity,

398   (Stevens et al., 2017) and is poorly expressed in the *Drosophila* midgut (see

399   http://flygutseq.buchonlab.com/ and https://flygut.epfl.ch/). However, Cry1A effects on

400   *Drosophila* progenitor cell fate appear to depend specifically on the DE-Cadherin present in the

401   adherens junctions, since overexpression of DE-Cadherin in progenitor cells (ISCs, EBs and EEPs)

402   can overcome Cry1A-induced impacts while another component of the adherens junctions

13

403   (Connectin) cannot. Interestingly, the percentage of identity between the Cry1A binding regions

404   (CBRs) shared by the orthologs of Cadherin-type receptors in different susceptible lepidopteran

405   species ranges from 21% to 66% (Li et al., 2021; Shao et al., 2018). Hence, the presence of a well-

406   conserved primary consensus sequence within the CBRs cannot explain the specificity of binding.

407   In agreement, it has been recently shown in susceptible Lepidoptera that only two dipeptides within

408   the CBRs are essential for high-affinity binding of Cry1A to its Cadherin receptor (Liu et al.,

409   2018a). These two dipeptides are not conserved in the CBRs of the Bt-R orthologs in different

410   lepidopteran species targeted by Cry1A toxins (Li et al., 2021). These data suggest that binding of

411   Cry1A to the receptor relies more on a conserved conformation of the CBRs than on a conserved

412   primary sequence. In addition, alignment of the *Helicoverpa armigera* (a Cry1A susceptible

413   lepidopteran) CBR sequence (Gao et al., 2019) and the DE-Cadherin sequence between amino

414   acids   164   and   298   shows   24%   identity   and   47%   similarity   (using   BlastP,

415   https://blast.ncbi.nlm.nih.gov/). Altogether, these results support a possible binding of Cry1A

416   toxins to *Drosophila* intestinal DE-cadherins, although this could occur with a low affinity.

417   Susceptibility of lepidopteran larvae to CryA1 toxins relies on the presence of a secondary

418   receptor such as Alkaline phosphatases, Aminopeptidases N, or ABC transporters (Adang et al.,

419   2014; Gao et al., 2019; Li et al., 2020; Liu et al., 2018b). None of the orthologs of these receptors

420   has been shown to be strongly expressed in the *Drosophila* midgut (Li et al., 2021; Stevens et al.,

421   2017), which could explain why binding of Cry1A to DE-cadherins does not lead to the death of

422   adult *Drosophila*. Interestingly, in *Drosophila* larvae, heterologous expression of ABCC2 from

423   *Bombix mori* or *Plutella xylostella*, or Aminopeptidases N from *Manduca sexta* was sufficient to

424   induce Cry1A-dependent death (Gill and Ellar, 2002; Obata et al., 2015). Conversely, heterologous

425   expression of the *Bombix mori* Cadherin Bt-R receptor in *Drosophila* is not sufficient to induce

426   death upon exposure to Cry1A but strongly enhances death when co-expressed with BmABCC2

427   (Obata et al., 2015). Together, these data suggest that, in *Drosophila,* in the absence of a Cadherin

428   receptor displaying a high affinity to Cry1A toxin, endogenous Cadherins with reduced affinity

429   toward Cry1A could step in to enhance the death potential of Cry1A toxins in the context of

430   heterologous expression of a secondary receptor from susceptible Lepidoptera. In agreement, it

431   has been previously demonstrated in *Drosophila* larvae that increasing the dose of ingested *Btk*

432   spores and crystals could ultimately lead to death (Babin et al., 2020; Cossentine et al., 2016),

433　arguing that the receptors (i.e., the Cadherins and the secondary receptors) present in the

434　*Drosophila* midgut have lower affinities for Cry1A toxins.

435　　　　Cry toxin activities in susceptible organisms rely not only on the presence of specific host

436　receptors in the midgut, but also on the extreme midgut pH and reducing environment allowing

437　crystal solubilization, as well as the enzymatic capacity of digestive proteins, both of which are

438　involved in the conversion of protoxins into active toxins (Fiuza et al., 2017; Mendoza-Almanza

439　et al., 2020; Pardo-López et al., 2013; Shao et al., 2013). Nevertheless, our data along with another

440　recent study (Stevens et al., 2017) suggest that crystals can be solubilized and then protoxins

441　activated in the *Drosophila* midgut. Therefore, more investigations will be necessary to understand

442　how crystals are processed and protoxins activated in the intestine of non-susceptible organisms.

443　What makes the difference between Cry-susceptible and non-susceptible organisms is likely the

444　affinity of Cry toxins for midgut host receptors. The higher the affinity of the toxins, the greater

445　the cellular damage/death and the greater the risk of death. In addition, the capacity of regeneration

446　of the midgut epithelium also plays an important role to overcome *Bt* pathogenicity (Castagnola

447　and Jurat-Fuentes, 2016). If the regeneration of the intestinal epithelium is more efficient than the

448　destructive capacity of Cry toxins, the host will survive. However, whatever the host is (susceptible

449　or non-susceptible), *Bt* uses a three-pronged strategy to improve its degree of virulence. First, it

450　tries to disrupt the epithelial barrier function by damaging or killing ECs. Second, it diverts the

451　behavior of the progenitor cells toward the wrong fate, thus limiting the amount of ECs produced

452　that are necessary to replace the damaged ones and to maintain the midgut integrity. Third, killing

453　ECs also reduces the capacity of these cells to produce reactive oxygen species and antimicrobial

454　peptides known to be involved in antimicrobial defenses (Allaire et al., 2018; Capo et al., 2016;

455　Kim and Lee, 2014).

456　　　　The *Bt* subspecies *kurstaki* and *aizawai* are widely used as microbial pesticide to fight

457　lepidopteran pests worldwide (Casida and Bryant, 2017), both subspecies partially producing the

458　same Cry1A toxins (Caballero et al., 2020). Likewise, 180 millions of hectares of genetically

459　modified crops express Cry1A toxins. Consequently, Cry1A toxins are present in the food, the

460　feed and in the environment, implying that many organisms might be affected. As the mechanisms

461　of intestinal progenitor fate choice are conserved in the animal kingdom (Guo et al., 2021; Joly

462　and Rousset, 2020; Zwick et al., 2019), it would be interesting to investigate whether Cry1A toxins

463　can also promote an increased number of EECs in other organisms (vertebrates and invertebrates).

464   EECs, through the production of neuropeptides and hormones, are involved in the regulation of

465   many physiological functions such as feeding behavior, metabolism and immune response (Guo

466   et al., 2021; Nässel and Zandawala, 2019; Watnick and Jugder, 2019). Consequences of this

467   increase in EEC number could be, for example, metabolic dysfunctions or inflammatory

468   pathologies. More studies are needed to understand the physiological impacts of this change in

469   intestinal cellular composition on organismal health.

Materials and Methods

470

Bacterial Strains

471

472    $Btk^{\Delta Cry}$ (identified under the code 4D22, (Gonzalez et al., 1982)), Btk^{Cry1Ac} (identified under the

473   code 4D4), and the *E. Coli* strains producing Cry1Ac (identified under the code ECE53), Cry1Ab

474   (identified under the code ECE54) and Cry2Aa (identified under the code ECE126) were obtained

475   from the Bacillus Genetic Stock Center (www.bgsc.org). The strain *Btk* SA-11 (Btk^{SA11}) was

476   isolated from the commercial product Delfin.

Generation of Btk^{Cry1Ab}

477

478   The mutant Btk^{Cry1Ab} producing only Cry1Ab as crystal toxin was obtained from the WT strain

479   Btk^{SA11}, by a procedure of plasmid curing, as follows. After isolation on TSA-YE agar

480   (Biomérieux, 18h culture at 30°C), the strain Btk^{SA11} was sub-cultured successively 3 times in 10ml

481   of brain heart Infusion (BHI, Oxoid) broth at 42°C with agitation, for 64, 48 and 36h respectively.

482   The first BHI culture was inoculated from an isolated colony, and the subsequent cultures were

483   inoculated with 100 µl of the previous ones. Clones from the last culture were isolated on TSA-

484   YE agar after serial dilution, then subcultured on the sporulating medium hydrolysate of casein

485   tryptone (HCT) + 0.3% Glc, in order to verify the absence of crystal production. Initially seeking

486   to select clones totally free of cry genes, we fortuitously selected partial mutants, including this

487   strain for which the single presence of *cry1Ab* as *cry* toxin gene, could be confirmed after WGS

488   analysis, as follows. The genomic DNA of Btk^{Cry1Ab} and *Btk* Btk^{SA11} was extracted using the

489   KingFisher cell and Tissue DNA kit (ThermoFisher) and sequenced using Illumina technology at

490   the Institut du Cerveau et de la Moelle Epinière (ICM) platform, as previously described (Bonis et

491   al., 2021), (NCBI accession numbers SAMN23436140 and SAMN23455549, respectively). The

492   absence of *cry* genes in Btk^{Cry1Ab}, with the exception of *cry1Ab,* was confirmed from raw reads

493   using KMA (Clausen et al., 2018).

16

Spore production

494

495 From isolated colonies on LB agar Petri dish, 4 x 5mL of *Bt* pre-culture was carried out. The pre-

496 culture was used for sowing 4 x 500mL of PGSM medium (0.75% casamino acids, 0.34% KH_2PO_4,

497 0.435% K_2HPO_4, 0.75% glucose, 1.25mM $CaCl_2$, 0.123% $MgSO_4$, 0.002% $MnSO_4$, 0.014%

498 $ZnSO_4$, 0.02% $FeSO_4$) and allowed to grow and sporulate in an incubator shaker at 30°C, 180 rpm

499 for 2 weeks. In order to eliminate vegetative cells, culture was heated 1 hour at 70°C and then

500 centrifuged 15 min at 7500g. The pellet was resuspended with a Dounce homogenizer in 1L of

501 150 mM NaCl and placed for 30 min on roller agitation at room temperature. After centrifugation

502 (15 min, 7500g), the pellet was washed twice with sterile water. The final pellet was resuspended

503 in 30mL of sterile water, dispatched in 1mL weighed tubes and lyophilized for 24-48h. The spore

504 mass was determined by the difference between the full and the empty tubes' weights.

Spore titer

505

506 The lyophilized spores were resuspended in sterile water to obtain a concentration of 50 mg/ml.

507 This solution was diluted serially (100µl in 900 µl of sterile water) to obtain 10^{-1} to 10^{-9} dilutions.

508 100 µl of dilutions 10^{-5} to 10^{-9} were plated on LB agar and incubated at 30°C overnight. The

509 number of colonies was counted for each dilution and reported to the mass of spores plated. The

510 experience was renewed three times. The mean of these ratios allows us to determine the titer of

511 spores in CFU (colony forming unit)/g.

Crystal purification

512

513 2x1g of *Btk*^{SA11} lyophilized spores were resuspended in 2 x 30 mL of sterile water and placed on

514 roller agitation at 4°C for 5h. Then, the solution was sonicated for 4 cycles of 15 sec/15 sec with

515 a frequency of 50% (Fisherbrand™ Model 505 Sonic Dismembrator). 6 x 10 mL were deposited

516 on a discontinuous sucrose gradient (67%/72%/79%) and centrifuged overnight in SW28 swinging

517 buckets at 100 000g at 4°C (ultracentrifuge Thermo-Sorval WX Ultra 80). The crystals were

518 collected at the 72%/79% and 72% /67% interfaces with a micropipette and dispatched by 10 mL

519 in centrifuge tubes (Beckman Avanti JE, rotor JA 25.50). 25 mL of sterile water were added in

520 each tube, vortexed and centrifuged at 4°C at 16 000g for 15 min. Each pellet was resuspended

521 with 20 mL of sterile water and centrifuged again in the same conditions. Each final pellet was

522 resuspended in 2 mL of sterile water, aliquoted by 1ml in weighed microtubes and lyophilized

17

523 24h-48h. The crystal mass was determined by the difference between the full and the empty tubes'
524 weights.

Cry protoxin production

526 2 x 15 mL of LB ampicillin (50mg/mL) were inoculated with two colonies of *E. Coli* expressing
527 the desired Cry toxin, and allowed to grow at 37°C, 220 rpm overnight. 4 x 5 mL of the overnight
528 preculture were added to 4 x 500 mL of LB ampicillin (50mg/mL) and allowed to grow at 37°C
529 and 200rpm until DO_{600}=0,6-0,7. Cry protein expression was induced by adding 500 µL of 1M
530 IPTG in each culture. The cultures were left at 37°C and 200rpm overnight and then centrifuged
531 at 6500g, 15 min at 22°C. Pellets were pooled in two batches and resuspended 100 mL of cold
532 WASH buffer (20mM Tris, 10mM EDTA, 1% Triton X-100, pH 7,5) and incubated 5 min at 4°C.
533 500 µL of lysozyme (20mg/mL) were added in each solution and incubated 15 min at 30°C and
534 then 5 min at 4°C. The solutions were sonicated for 6 cycles of 15 sec/15 sec' at 40%
535 (Fisherbrand™ Model 505 Sonic Dismembrator) and centrifuged 10 min at 10 000g, at 4°C. The
536 pellets were washed twice with 100ml of WASH buffer and centrifuged in the same conditions.
537 The last pellets were weighed, resuspended in CAPS buffer (50mM CAPS, 0,3% lauroyl-
538 sarcosine, 1mM DTT pH11) to obtain a final concentration of 100mg/mL, placed for 30 min under
539 roller agitation at room temperature and centrifuged 10 min at 10 000g, 4°C. The supernatant was
540 dialyzed twice against 50 volume of PBS1x, 0,1mM DTT and twice against 50 volume of PBS1x
541 at 4°C and centrifuged 10 min at 20 000g at 4°C. The supernatant was conserved at -20°C until
542 purification or digestion (activation) by trypsin.

Cry toxin activation

544 Half of the produced supernatant (see above) was dosed by the Bradford method (Protein Assay
545 Dye Reagent Concentrate, Biorad #500-0006) and digested with 1% trypsin (weight/weight)
546 (Trypsin from bovine pancreas, Sigma #T1005) at 37°C for 72h. The Cry toxins were then purified
547 by FPLC. NB: After 72h, the trypsin is fully degraded.

Cry toxin purification

549 The Cry toxins produced from *E.Coli* (activated or not) were purified by FPLC (Äkta,
550 UPC900/P920/INV907/FRAC950) on a 1 mL benzamidine column (HiTrap^{TM} Benzamidine FF
551 (high sub), GE Healthcare #17-5143-01) with PBS1X as charge buffer, PBS1x, 1M NaCl as buffer
552 for non-specific link and 100mM glycin pH3 as elution buffer.

18

Fly Stocks and Genetics

The following stocks are listed at the Bloomington *Drosophila* Stock Center (https://bdsc.indiana.edu/): WT canton S (#64349). *w; Sco/CyO; tub-GAL80^{ts}/TM6b* (#7018). *w; tub-GAL80^{ts}; TM2/TM6b* (#7019). *w; esg-GAL4^{NP5130}* (#67054). *w; UAS-GFP/TM3 Sb* (#5430). *w; UAS-shg-R* (DE-Cadherin)(#58494); *y w, shg::Tomato* (#58789).

Other stocks: *w; ; Dl-GAL4/TM6b* (Zeng et al., 2010). *w; tub-GAL80^{ts}; Dl-GAL4 UAS-GFP/TM6b* (this study). *w; esg-GAL4^{NP5130} UAS-GFP* (Shaw et al., 2010). *w; esg-GAL4^{NP5130} UAS-GFP; tubGAL80^{ts}* (Apidianakis et al., 2009). *w; Su(H)GBE-GAL4, UAS-CD8::GFP* (Zeng et al., 2010). *w; Su(H)GBE-GAL4/SM6β; tub-GAL80^{ts} UAS-GFP/TM6b* (this study). *w; myo1A-GAL4* (Shaw et al., 2010). *w; myo1A-GAL4 UAS-GFP/CyO* (Apidianakis et al., 2009). *w; UAS-GFP::CD8; UAS-H2B::RFP/TM2* (Antonello et al., 2015). *w; UAS-CD8::GFP; UAS-H2B::RFP, tub-GAL80^{ts}/TM2* (Antonello et al., 2015). *w; esg-GAL4, UAS-CD8::GFP; UAS-H2B::RFP, tub-GAL80^{ts}/TM6b* (Antonello et al., 2015). *w; UAS-CD8::GFP; Dl-GAL4, UAS-H2B::RFP/TM6b* (this study). *w; ; UAS-GC3Ai^{G7S} (UAS-Casp::GFP)* (Schott et al., 2017). *w; UAS-connectin* (Zhai et al., 2017).

Cell lineage

<u>*Dl-ReDDM* experiments</u>: *w; tub-GAL80^{ts}; Dl-GAL4 UAS-GFP/TM6b* females were crossed to *w; UAS-GFP::CD8; UAS-H2B::RFP/TM6* males at 18°C. Progeny were kept at 18°C until emergence. Flies were transferred at 25°C for 5 days before infection, and then transferred at 29°C for 2 days (Figure S1B).

<u>*esg-ReDDM* experiments</u>: *w; esg-GAL4 UAS-GFP; UAS-H2B::RFP, tub-GAL80^{ts}/TM6b* females were crossed to WT males at 18°C. Progeny were kept at 18°C until emergence. Flies were transferred at 25°C for 5 days before infection, and then transferred at 29°C for 3 days (Figure3).

<u>*Su(H)-ReDDM* experiments</u>: *w; Su(H)-GAL4/SM6β; tub-GAL80^{ts} UAS-GFP/TM6b* female*s* were crossed to *w; UAS-GFP::CD8; UAS-H2B::RFP/TM6* males at 18°C. Progeny were kept at 18°C until emergence. Flies were transferred at 25°C for 5 days before infection, and then transferred at 29°C for 3 days (Figure S3).

<u>DE-Cadherin and Connectin overexpression</u>: *w; esg-Gal4 UAS-GFP; UAS-H2B::RFP, tub-GAL80^{ts}/TM6b* females were crossed to *UAS-DE-Cadherin* males. Progeny were kept at 18°C until emergence. Flies were transferred at 25°C for 5 days before infection, and then transferred at 29°C for 3 days (Figure 5 and S5).

583 *Drosophila rearing and oral infection*

584 *Drosophila* were reared on standard medium (0.8% Agar, 2.5% sugar, 8% corn flour, 2% yeast) at

585 25 ° C with a 12h light/12h dark cycle. For oral infection, after 2 h of starvation to synchronize the

586 food intake, ten 5 to 6 day-old non-virgin females were transferred onto a fly medium vial covered

587 with a filter disk soaked with water (control) or a suspension of spores, (corresponding to 10^6 CFU

588 of spores per 4 cm² and per individual female (Loudhaief et al., 2017; Nawrot-Esposito et al.,

589 2020)), crystals, protoxin or activated toxins. The quantity of crystals, protoxin or activated toxins

590 deposited on the filter disc corresponded to 30% of the spore weight, *Btk* crystals representing

591 between 25% and 30% of the total weight of the 1:1 spore/crystal mix (Agaisse and Lereclus;

592 1995; Monroe, (1961); Murty et al., 1994). Flies were kept feeding on the contaminated media

593 until dissection in all the experiments.

594 *Dissection, immunostaining and microscopy*

595 Dissection, fixation and immunostaining were performed as described by (Micchelli, 2014).

596 Dilutions of the various antibodies were: mouse anti-Armadillo N27A1 at 1:50 (DSHB), mouse

597 anti-Connectin-C1-427 at 1/200 (DSHB), mouse anti-Prospero MR1A at 1:200 (DSHB), rabbit

598 anti-PH3 at 1:1000 (Millipore, 06-570), Rabbit anti-Cleaved Caspase-3 at 1/600 (Cell Signalling

599 Asp175 #9661), Goat anti-mouse AlexaFluor-647 at 1/500 (Molecular Probes Cat# A-21235),

600 Goat anti mouse AlexaFluor-546 at 1/500 (Molecular Probes Cat# A-11003), Goat anti-rabbit

601 AlexaFluor-647 at 1/500 (Thermo Fisher Scientific Cat# A32733), Goat anti-rabbit AlexaFluor-

602 546 at 1/500 (Thermo Fisher Scientific Cat# A-11010). For microscopy, guts were mounted in

603 Fluoroshield DAPI medium (Sigma, # F6057) and immediately observed on a Zeiss Axioplan Z1

604 with Apotome 2 microscope. Images were analyzed using ZEN (Zeiss), ImageJ and Photoshop

605 software. Image acquisition was performed at the microscopy platform of the Sophia Agrobiotech

606 Institute (INRAE1355-UCA-CNRS7254 – Sophia Antipolis).

607 *DNA constructs*

608 The full-length expression construct of DE-cadherin Full Length fused to GFP (DEFL) was

609 introduced into pUAST as previously described (Oda and Tsukita, 1999).

610 *Cell aggregation assay*

611 *Drosophila* Schneider 2 (S2) cells were cultured in Schneider's medium supplemented with 10%

612 heat-inactivated fetal bovine serum (FBS) at 25°C in a non-humidified ambient air-regulated

20

613   incubator. For S2 aggregation assay, 2.2 10^6 cells were plated in 25 cm^2 flask for each condition.

614   After 6 h, transient transfection was performed by mixing transfection reagent (TransIT®-2020;

615   Mirus Bio) with a reagent-to-DNA ratio of 3:1. A total of 3 µg plasmid DNA per T25 was used,

616   corresponding to a 5:1 mixture of pUAST-DEFL and pWA-GAL4. Approximately 46h after

617   transfection, the cells were collected into 15 mL tubes and centrifuged for 5 minutes at 400 g. The

618   pellet was resuspended in 2 ml of fresh medium supplemented in CaCl$_2$ to obtain a final

619   concentration of 7.4 mM and separated into single cells by repeated pipetting. 500 µL of this cell

620   suspension were added to a well of a 24-well microplate. To allow cell-cell adhesion (aggregation),

621   the microplate was placed under constant agitation on a rotary platform at 150 rpm at 25°C for the

622   indicated time (1h, 2h and 3h) with or without protoxins (at a final concentration 35µg/ml). Cell

623   aggregates formed in the wells were observed using an inverted Fluorescent microscope (Nikon,

624   Eclipse TE2000-U). Images for the florescence of GFP was acquired using a CCD camera (ORCA

625   ER, Hamamatsu Photonics). The same parameter settings were used to acquire images (objectives,

626   gain, exposure time …). The area of fluorescent aggregates and individual cells were measured

627   using Fiji software (Schindelin et al., 2012). The average area of a S2 cell in our condition is about

628   15.5 µm^2. Hence, quantification of the aggregates area was performed excluding all objects smaller

629   than 15 µm^2. The mean area of aggregates were calculated after background subtraction. Three

630   independent experiments were performed for each condition. Values in µm^2 were represented in

631   GraphPad Prism 5 software as scatter-plot view. Statistical analysis was conducted using

632   GraphPad Prism 5 software. The significance of the difference between CTR and exposed

633   conditions was assessed using one-way ANOVA and Tukey's post hoc tests. Statistical parameters

634   for each experiment can be found within the corresponding figure legends.

635   ***Western blot***

636   Figure 6D: Twenty *Drosophila* (5 to 6 day-old non-virgin females) were orally infected with

637   spores and reared at 25°C with a 12h/12h day/night cycle for the indicated time. At the same time,

638   10^7 CFU of spores in 50µl of sterile water were incubated in the same conditions. After 4, 24, 72

639   or 144h, *Drosophila* midguts were dissected in PBS1x with anti-proteases (cOmplete Tablets

640   EDTA free EASY Pack, Roche #04693132001). Then midguts were transferred on ice into a 2 ml

641   microtube containing 200 µL of PBS1x with anti-proteases and crushed one minute at 30Hz with

642   a Tissue Lyser (Qiagen, Tissue Lyser LT).

643   Figure 6E: Twenty *Drosophila* (5 to 6 day-old non-virgin females) were orally infected with water

644   or purified crystals and reared at 25°C with a 12h/12h day/night cycle for the indicated time. Flies

645   were dissected and anterior and posterior regions of midguts were separated and lysed in a

646   hypotonic buffer (25 mM HEPES, pH 7.5, 5 mM $MgCl_2$, 5 mM EDTA, 5 mM DTT, 2 mM PMSF,

647   10 µg/mL leupeptin, 10 µg/mL pepstatin A) on ice. Midguts were crushed one minute at 30 Hz

648   with the Tissue Lyser. Homogenates were centrifuged at 20 000 g for 45 min at 4°C. The

649   supernatant was the soluble fraction (considered as cytosol-enriched fraction) and the pellet was

650   the insoluble fraction (containing membranes).

651   Proteins were dosed by Bradford method (Protein Assay Dye Reagent Concentrate, Biorad #500-

652   0006). 20µg of midgut proteins and 2.10^4 CFU of spores were deposited on a 8.5% SDS-

653   polyacrylamide gel. After migration at 100V for 1h30, proteins were transferred onto a PVDF

654   membrane (Immobilon®-P Membrane, Millipore #IPVH00010) (120mA/gel, 1h) in a semi-dried

655   transfer system with a transfer buffer (200 mM glycine, 25 mM Tris base, 0,1% SDS, pH7,4, 20%

656   methanol). Membranes were saturated with 5% milk in TBS-T (140mM NaCl, 10 mM Tris base,

657   0,1% Tween 20, pH 7.4) for 1h and incubated overnight at 4°C with a homemade anti-Cry1A

658   antibody (Babin et al., 2020) diluted at 1/7 500 in TBS-T 3% BSA. After three rinsings of 10 min

659   each with TBST, membranes were incubated with an anti-rabbit antibody coupled with HRP (Goat

660   Anti-Rabbit (IgG), Invitrogen #G21234) diluted 1/7 500 in TBS-T 2% milk for 1 hour at room

661   temperature. Membranes were rinsed three times with TBST and once with TBS. Western blots

662   were revealed with enhanced chemiluminescence (luminol and hydrogen peroxide, homemade) on

663   an autoradiographic film (Amersham Hyperfilm™ ECL, GE Healthcare #28906837).

664   ***Measurement, counting and statistical analysis***

665   In all the data presented, the pictures and counting were always performed in the posterior part of

666   the R4 region (http://flygut.epfl.ch/) named R4bc in the flygut site (see also (Buchon et al., 2013;

667   Marianes and Spradling, 2013)). Experiments were independently repeated at least three times.

668   Cells were counted in a fixed area (20.000 µm²) within the R4bc region. Effects of treatments were

669   analyzed using a Kyplot (KP test). Differences were considered significant when P<0.05 (*P≤0.05,

670   **P≤0.01, ***P≤0.001).

671

Acknowledgments

Author contributions

RJ: Conceptualization, Data curation, Formal analysis, Investigation, Visualization, Writing – original draft

RL: Conceptualization, Investigation, Visualization

NZP: Formal Analysis, Investigation, Visualization

MPNE: Methodology

AF: Formal Analysis, Data curation

RR: Funding acquisition, Validation, Writing – review & editing

MB: Methodology, Resources, Data curation,

DO: Conceptualization, Funding acquisition, Validation, Writing – review & editing

AG: Conceptualization, Data curation, Formal Analysis, Data curation, Funding acquisition, Project administration, Supervision, Validation, Visualization, Writing – review & editing

Funding

705 **Bibliography**

706 Adang, M.J., Crickmore, N. and Jurat-Fuentes, J.L. (2014) Chapter Two – Diversity of Bacillus thuringiensis
707   Crystal Toxins and Mechanism of Action. *Advances in Insect Physiology*, **47**, 39–87.
708 Allaire, J.M., Crowley, S.M., Law, H.T., Chang, S.Y., Ko, H.J. and Vallance, B.A. (2018) The Intestinal
709   Epithelium: Central Coordinator of Mucosal Immunity. *Trends Immunol*, **39**, 677-696.
710 Antonello, Z.A., Reiff, T., Ballesta-Illan, E. and Dominguez, M. (2015) Robust intestinal homeostasis relies
711   on cellular plasticity in enteroblasts mediated by miR-8-Escargot switch. *EMBO*, **34**, 2025-2041.
712   doi: 2010.15252/embj.201591517. Epub 201592015 Jun 201591515.
713 Apidianakis, Y., Pitsouli, C., Perrimon, N. and Rahme, L. (2009) Synergy between bacterial infection and
714   genetic predisposition in intestinal dysplasia. *Proc Natl Acad Sci U S A*, **106**, 20883-20888. Epub
715   22009 Nov 20823.
716 Babin, A., Nawrot-Esposito, M.-P., Gallet, A., Gatti, J.-L. and Poirié, M. (2020) Differential side-effects of
717   Bacillus thuringiensis bioinsecticide on non-target Drosophila flies. *Scientific Reports*, **10**, 16241.
718 Beehler-Evans, R. and Micchelli, C.A. (2015) Generation of enteroendocrine cell diversity in midgut stem
719   cell lineages. *Development*, **142**, 654-664. doi: 610.1242/dev.114959.
720 Biggel, M., Etter, D., Corti, S., Brodmann, P., Stephan, R., Ehling-Schulz, M. and Johler, S. (2021) Whole
721   Genome Sequencing Reveals Biopesticidal Origin of Bacillus thuringiensis in Foods. *Front*
722   *Microbiol*, **12**, 775669.
723 Biteau, B., Hochmuth, C.E. and Jasper, H. (2008) JNK activity in somatic stem cells causes loss of tissue
724   homeostasis in the aging Drosophila gut. *Cell Stem Cell*, **3**, 442-455.
725 Biteau, B. and Jasper, H. (2014) Slit/Robo Signaling Regulates Cell Fate Decisions in the Intestinal Stem Cell
726   Lineage of Drosophila. S2211-1247(2214)00399-00394. doi:
727   00310.01016/j.celrep.02014.00305.00024.
728 Bonfini, A., Liu, X. and Buchon, N. (2016) From pathogens to microbiota: How Drosophila intestinal stem
729   cells react to gut microbes. S0145-0305X(0116)30032-30035. doi:
730   30010.31016/j.dci.32016.30002.30008.
731 Bonis, M., Felten, A., Pairaud, S., Dijoux, A., Maladen, V., Mallet, L., Radomski, N., Duboisset, A., Arar, C.,
732   Sarda, X., Vial, G., Mistou, M.Y., Firmesse, O., Hennekinne, J.A. and Herbin, S. (2021) Comparative
733   phenotypic, genotypic and genomic analyses of Bacillus thuringiensis associated with foodborne
734   outbreaks in France. *PLoS One*, **16**, e0246885.
735 Brand, A.H. and Perrimon, N. (1993) Targeted gene expression as a means of altering cell fates and
736   generating dominant phenotypes. *Development*, **118**, 401-415.
737 Buchon, N., Osman, D., David, F.P., Fang, H.Y., Boquete, J.P., Deplancke, B. and Lemaitre, B. (2013)
738   Morphological and molecular characterization of adult midgut compartmentalization in
739   Drosophila. *Cell Rep*, **3**, 1725-1738. doi: 1710.1016/j.celrep.2013.1704.1001. Epub 2013 May
740   1722.
741 Caballero, J., Jiménez-Moreno, N., Orera, I., Williams, T., Fernández, A.B., Villanueva, M., Ferré, J.,
742   Caballero, P. and Ancín-Azpilicueta, C. (2020) Unraveling the Composition of Insecticidal Crystal
743   Proteins in Bacillus thuringiensis: a Proteomics Approach. *Appl Environ Microbiol.*, **86**, e00476-
744   00420. doi: 00410.01128/AEM.00476-00420. Print 02020 Jun 00472.

745   Capo, F., Charroux, B. and Royet, J. (2016) Bacteria sensing mechanisms in Drosophila gut: Local and
746   systemic consequences. *Dev Comp Immunol*, **64:11-21.**, 10.1016/j.dci.2016.1001.1001. Epub
747   2016 Jan 1018.
748   Casida, J.E. and Bryant, R.J. (2017) The ABCs of pesticide toxicology: amounts, biology, and chemistry.
749   *Toxicol Res (Camb).* **6**, 755-763. doi: 710.1039/c1037tx00198c. eCollection 02017 Nov 00191.
750   Castagnola, A. and Jurat-Fuentes, J.L. (2016) Intestinal regeneration as an insect resistance mechanism to
751   entomopathogenic bacteria. *Curr Opin Insect Sci.*, **15:104-10.**, 10.1016/j.cois.2016.1004.1008.
752   Epub 2016 Apr 1020.
753   Castella, C., Pauron, D., Hilliou, F., Trang, V.T., Zucchini-Pascal, N., Gallet, A. and Barbero, P. (2019)
754   Transcriptomic analysis of Spodoptera frugiperda Sf9 cells resistant to Bacillus thuringiensis
755   Cry1Ca toxin reveals that extracellular Ca(2+), Mg(2+) and production of cAMP are involved in
756   toxicity. *Biol Open.*, **8(4).** bio.037085. doi: 037010.031242/bio.037085.
757   Chatterjee, M. and Ip, Y.T. (2009) Pathogenic stimulation of intestinal stem cell response in Drosophila. *J
758   Cell Physiol*, **220**, 664-671. doi: 610.1002/jcp.21808.
759   Choi, N.H., Lucchetta, E. and Ohlstein, B. (2011) Nonautonomous regulation of Drosophila midgut stem
760   cell proliferation by the insulin-signaling pathway. *Proc Natl Acad Sci U S A*, **108**, 18702-18707.
761   doi: 18710.11073/pnas.1109348108. Epub 1109342011 Nov 1109348102.
762   Clausen, P., Aarestrup, F.M. and Lund, O. (2018) Rapid and precise alignment of raw reads against
763   redundant databases with KMA. *BMC Bioinformatics*, **19**, 307.
764   Cossentine, J., Robertson, M. and Xu, D. (2016) Biological Activity of Bacillus thuringiensis in Drosophila
765   suzukii (Diptera: Drosophilidae). *J Econ Entomol*, **22**.
766   de Navascues, J., Perdigoto, C.N., Bian, Y., Schneider, M.H., Bardin, A.J., Martinez-Arias, A. and Simons,
767   B.D. (2012) Drosophila midgut homeostasis involves neutral competition between symmetrically
768   dividing intestinal stem cells. *EMBO J*, **31**, 2473-2485. doi: 2410.1038/emboj.2012.2106. Epub
769   2012 Apr 2420.
770   Ehling-Schulz, M., Lereclus, D. and Koehler, T.M. (2019) The Bacillus cereus Group: Bacillus Species with
771   Pathogenic Potential. *Microbiol Spectr.*, **7(3).** 10.1128/microbiolspec.GPP1123-0032-2018.
772   Falo-Sanjuan, J. and Bray, S.J. (2021) Membrane architecture and adherens junctions contribute to strong
773   Notch pathway activation. *Development*, **148**.
774   Fiuza, L.M., Polanczyk, R.A. and Crickmore, N. (2017) *Bacillus thuringiensis and Lysinibacillus sphaericus:
775   Characterization and use in the field of biocontrol*. Springer.
776   Gao, M., Dong, S., Hu, X., Zhang, X., Liu, Y., Zhong, J., Lu, L., Wang, Y., Chen, L. and Liu, X. (2019) Roles of
777   Midgut Cadherin from Two Moths in Different Bacillus thuringiensis Action Mechanisms:
778   Correlation among Toxin Binding, Cellular Toxicity, and Synergism. *J Agric Food Chem*, **67**, 13237-
779   13246.
780   Gill, M. and Ellar, D. (2002) Transgenic Drosophila reveals a functional in vivo receptor for the Bacillus
781   thuringiensis toxin Cry1Ac1. *Insect Mol Biol*, **11**, 619-625.
782   Glasset, B., Herbin, S., Guillier, L., Cadel-Six, S., Vignaud, M.L., Grout, J., Pairaud, S., Michel, V., Hennekinne,
783   J.A., Ramarao, N. and Brisabois, A. (2016) Bacillus cereus-induced food-borne outbreaks in France,
784   2007 to 2014: epidemiology and genetic characterisation. *Euro Surveill.*, **21(48).** 30413. doi:
785   30410.32807/31560-37917.ES.32016.30421.30448.30413.
786   Gonzalez, J.M., Jr., Brown, B.J. and Carlton, B.C. (1982) Transfer of Bacillus thuringiensis plasmids coding
787   for delta-endotoxin among strains of B. thuringiensis and B. cereus. *Proc Natl Acad Sci U S A*, **79**,
788   6951-6955.
789   Goulas, S., Conder, R. and Knoblich, J.A. (2012) The Par complex and integrins direct asymmetric cell
790   division in adult intestinal stem cells. *Cell Stem Cell*, **11**, 529-540. doi:
791   510.1016/j.stem.2012.1006.1017.

792   Grisolia, C.K., Oliveira, R., Domingues, I., Oliveira-Filho, E.C., Monerat, R.G. and Soares, A.M. (2009)
793   Genotoxic evaluation of different delta-endotoxins from Bacillus thuringiensis on zebrafish adults
794   and development in early life stages. *Mutat Res*, **672**, 119-123.
795   Guisoni, N., Martinez-Corral, R., Garcia-Ojalvo, J. and de Navascues, J. (2017) Diversity of fate outcomes
796   in cell pairs under lateral inhibition. *Development.*, **144**, 1177-1186. doi: 1110.1242/dev.137950.
797   Epub 132017 Feb 137957.
798   Guo, X., Lv, J. and Xi, R. (2021) The specification and function of enteroendocrine cells in Drosophila and
799   mammals: a comparative review. *Febs j*.
800   Guo, Z. and Ohlstein, B. (2015) Stem cell regulation. Bidirectional Notch signaling regulates Drosophila
801   intestinal stem cell multipotency. *Science*, **350(6263).** aab0988. doi: 0910.1126/science.aab0988.
802   Hernández-Rodríguez, C.S., Hernández-Martínez, P., Van Rie, J., Escriche, B. and Ferré, J. (2013) Shared
803   midgut binding sites for Cry1A.105, Cry1Aa, Cry1Ab, Cry1Ac and Cry1Fa proteins from Bacillus
804   thuringiensis in two important corn pests, Ostrinia nubilalis and Spodoptera frugiperda. *PLoS One*,
805   **8**, e68164.
806   Hill, E., Broadbent, I.D., Chothia, C. and Pettitt, J. (2001) Cadherin superfamily proteins in Caenorhabditis
807   elegans and Drosophila melanogaster. *J Mol Biol*, **305**, 1011-1024.
808   Hung, T.P., Truong, L.V., Binh, N.D., Frutos, R., Quiquampoix, H. and Staunton, S. (2016) Fate of insecticidal
809   Bacillus thuringiensis Cry protein in soil: differences between purified toxin and biopesticide
810   formulation. *Pest Manag Sci.*, **72**, 2247-2253. doi: 2210.1002/ps.4262.
811   ISAAA. (2017) Global Status of Commercialized Biotech/GM Crops in 2017: Biotech Crop Adoption Surges
812   as Economic Benefits Accumulate in 22 Years. ISAAA: Ithaca, NY.
813   Jiang, H., Patel, P.H., Kohlmaier, A., Grenley, M.O., McEwen, D.G. and Edgar, B.A. (2009) Cytokine/Jak/Stat
814   signaling mediates regeneration and homeostasis in the Drosophila midgut. *Cell*, **137**, 1343-1355.
815   doi: 1310.1016/j.cell.2009.1305.1014.
816   Johler, S., Kalbhenn, E.M., Heini, N., Brodmann, P., Gautsch, S., Bagcioglu, M., Contzen, M., Stephan, R.
817   and Ehling-Schulz, M. (2018) Enterotoxin Production of Bacillus thuringiensis Isolates From
818   Biopesticides, Foods, and Outbreaks. *Front Microbiol.*, **9:1915.**, 10.3389/fmicb.2018.01915.
819   eCollection 02018.
820   Joly, A. and Rousset, R. (2020) Tissue Adaptation to Environmental Cues by Symmetric and Asymmetric
821   Division Modes of Intestinal Stem Cells. *Int J Mol Sci*, **21**.
822   Jovanovic, J., Ornelis, V.F.M., Madder, A. and Rajkovic, A. (2021) Bacillus cereus food intoxication and
823   toxicoinfection. *Compr Rev Food Sci Food Saf*, **20**, 3719-3761.
824   Kim, S.H. and Lee, W.J. (2014) Role of DUOX in gut inflammation: lessons from Drosophila model of gut-
825   microbiota interactions. *Front Infect Microbiol.*, **3**, 116.
826   Li, Q., Li, M., Zhu, M., Zhong, J., Wen, L., Zhang, J., Zhang, R., Gao, Q., Yu, X.Q. and Lu, Y. (2021) Genome-
827   wide identification and comparative analysis of Cry toxin receptor families in 7 insect species with
828   a focus on Spodoptera litura. *Insect Sci*.
829   Li, Q., Li, S., Mana-Capelli, S., Roth Flach, R.J., Danai, L.V., Amcheslavsky, A., Nie, Y., Kaneko, S., Yao, X.,
830   Chen, X., Cotton, J.L., Mao, J., McCollum, D., Jiang, J., Czech, M.P., Xu, L. and Ip, Y.T. (2014) The
831   conserved misshapen-warts-Yorkie pathway acts in enteroblasts to regulate intestinal stem cells
832   in Drosophila. *Dev Cell*, **31**, 291-304. doi: 210.1016/j.devcel.2014.1009.1012. Epub 2014 Nov
833   1010.
834   Li, X., Miyamoto, K., Takasu, Y., Wada, S., Iizuka, T., Adegawa, S., Sato, R. and Watanabe, K. (2020) ATP-
835   Binding Cassette Subfamily A Member 2 is a Functional Receptor for Bacillus thuringiensis Cry2A
836   Toxins in Bombyx mori, but not for Cry1A, Cry1C, Cry1D, Cry1F, or Cry9A Toxins. *Toxins (Basel)*,
837   **12**.

838 Liu, L., Boyd, S.D., Bulla, L.A., Jr. and Winkler, D.D. (2018a) "The Defined Toxin-binding Region of the
839 Cadherin G-protein Coupled Receptor, BT-R(1), for the Active Cry1Ab Toxin of Bacillus
840 thuringiensis". *J Proteomics Bioinform*, **11**, 201-210.
841 Liu, M., Huang, R., Weisman, A., Yu, X., Lee, S.H., Chen, Y., Huang, C., Hu, S., Chen, X., Tan, W., Liu, F., Chen,
842 H. and Shea, K.J. (2018b) Synthetic Polymer Affinity Ligand for Bacillus thuringiensis (Bt)
843 Cry1Ab/Ac Protein: The Use of Biomimicry Based on the Bt Protein-Insect Receptor Binding
844 Mechanism. *J Am Chem Soc*, **140**, 6853-6864.
845 Loudhaief, R., Brun-Barale, A., Benguettat, O., Nawrot-Esposito, M.P., Pauron, D., Amichot, M. and Gallet,
846 A. (2017) Apoptosis restores cellular density by eliminating a physiologically or genetically induced
847 excess of enterocytes in the Drosophila midgut. *Development*, **144**, 808-819. doi:
848 810.1242/dev.142539.
849 Maeda, K., Takemura, M., Umemori, M. and Adachi-Yamada, T. (2008) E-cadherin prolongs the moment
850 for interaction between intestinal stem cell and its progenitor cell to ensure Notch signaling in
851 adult Drosophila midgut. *Genes Cells*, **13**, 1219-1227. doi: 1210.1111/j.1365-2443.2008.01239.x.
852 Epub 02008 Oct 01222.
853 Marianes, A. and Spradling, A.C. (2013) Physiological and stem cell compartmentalization within the
854 Drosophila midgut. *Elife*, **2:e00886.**, 10.7554/eLife.00886.
855 Mendoza-Almanza, G., Esparza-Ibarra, E.L., Ayala-Luján, J.L., Mercado-Reyes, M., Godina-González, S.,
856 Hernández-Barrales, M. and Olmos-Soto, J. (2020) The Cytocidal Spectrum of Bacillus
857 thuringiensis Toxins: From Insects to Human Cancer Cells. *Toxins (Basel)*, **12**.
858 Micchelli, C.A. (2014) Whole-mount immunostaining of the adult Drosophila gastrointestinal tract.
859 *Methods*, **68**, 273-279. doi: 210.1016/j.ymeth.2014.1003.1022. Epub 2014 Mar 1027.
860 Micchelli, C.A. and Perrimon, N. (2006) Evidence that stem cells reside in the adult Drosophila midgut
861 epithelium. *Nature*, **439**, 475-479. Epub 2005 Dec 2007.
862 Nässel, D.R. and Zandawala, M. (2019) Recent advances in neuropeptide signaling in Drosophila, from
863 genes to physiology and behavior. *Prog Neurobiol*, **179**, 101607.
864 Nawrot-Esposito, M.P., Babin, A., Pasco, M., Poirié, M., Gatti, J.L. and Gallet, A. (2020) Bacillus
865 thuringiensis Bioinsecticides Induce Developmental Defects in Non-Target Drosophila
866 melanogaster Larvae. *Insects*, **11**.
867 O'Brien, L.E., Soliman, S.S., Li, X. and Bilder, D. (2011) Altered modes of stem cell division drive adaptive
868 intestinal growth. *Cell*, **147**, 603-614. doi: 610.1016/j.cell.2011.1008.1048.
869 Obata, F., Tanaka, S., Kashio, S., Tsujimura, H., Sato, R. and Miura, M. (2015) Induction of rapid and
870 selective cell necrosis in Drosophila using Bacillus thuringiensis Cry toxin and its silkworm
871 receptor. *BMC Biol*, **13**, 48.
872 Oda, H. and Tsukita, S. (1999) Nonchordate classic cadherins have a structurally and functionally unique
873 domain that is absent from chordate classic cadherins. *Dev Biol*, **216**, 406-422.
874 Ohlstein, B. and Spradling, A. (2006) The adult Drosophila posterior midgut is maintained by pluripotent
875 stem cells. *Nature*, **439**, 470-474. Epub 2005 Dec 2007.
876 Ohlstein, B. and Spradling, A. (2007) Multipotent Drosophila intestinal stem cells specify daughter cell
877 fates by differential notch signaling. *Science*, **315**, 988-992.
878 Osman, D., Buchon, N., Chakrabarti, S., Huang, Y.T., Su, W.C., Poidevin, M., Tsai, Y.C. and Lemaitre, B.
879 (2012) Autocrine and paracrine unpaired signaling regulate intestinal stem cell maintenance and
880 division. *J Cell Sci*, **125**, 5944-5949. doi: 5910.1242/jcs.113100. Epub 112012 Oct 113104.
881 Pardo-Lopez, L., Soberon, M. and Bravo, A. (2012) Bacillus thuringiensis insecticidal three-domain Cry
882 toxins: mode of action, insect resistance and consequences for crop protection. *FEMS Microbiol*
883 *Rev*, **37**, 3-22. doi: 10.1111/j.1574-6976.2012.00341.x. Epub 02012 Jun 00311.

884   Pardo-López, L., Soberón, M. and Bravo, A. (2013) Bacillus thuringiensis insecticidal three-domain Cry
885   toxins: mode of action, insect resistance and consequences for crop protection. *FEMS Microbiol*
886   *Rev*, **37**, 3-22.
887   Pasco, M.Y., Loudhaief, R. and Gallet, A. (2015) The cellular homeostasis of the gut: what the Drosophila
888   model points out. *Histol Histopathol.*, **Vol 30**, pp 277-292.
889   Perdigoto, C.N. and Bardin, A.J. (2013) Sending the right signal: Notch and stem cells. *Biochim Biophys*
890   *Acta*, **1830**, 2307-2322. doi: 2310.1016/j.bbagen.2012.2308.2009. Epub 2012 Aug 2316.
891   Rabinovitch, L., Vivoni, A.M., Machado, V., Knaak, N., Berlitz, D.L., Polanczyk, R.A. and Fiuza, L.M. (2017)
892   Bacillus thuringiensis Characterization: Morphology, Physiology, Biochemistry, Pathotype,
893   Cellular, and Molecular Aspects. In Fiuza, L.M., Polanczyk, R.A. and Crickmore, N. (eds.), *Bacillus*
894   *thuringiensis and Lysinibacillus sphaericus*. Springer International Publishing, pp. 1-18.
895   Rosi-Marshall, E.J., Tank, J.L., Royer, T.V., Whiles, M.R., Evans-White, M., Chambers, C., Griffiths, N.A.,
896   Pokelsek, J. and Stephen, M.L. (2007) Toxins in transgenic crop byproducts may affect headwater
897   stream ecosystems. *Proc Natl Acad Sci U S A*, **104**, 16204-16208.
898   Rubio-Infante, N. and Moreno-Fierros, L. (2016) An overview of the safety and biological effects of Bacillus
899   thuringiensis Cry toxins in mammals. *J Appl Toxicol*, **36**, 630-648. doi: 610.1002/jat.3252. Epub
900   2015 Nov 1004.
901   Sallé, J., Gervais, L., Boumard, B., Stefanutti, M., Siudeja, K. and Bardin, A.J. (2017) Intrinsic regulation of
902   enteroendocrine fate by Numb. *The EMBO Journal*, **36**, 1928-1945.
903   Schindelin, J., Arganda-Carreras, I., Frise, E., Kaynig, V., Longair, M., Pietzsch, T., Preibisch, S., Rueden, C.,
904   Saalfeld, S., Schmid, B., Tinevez, J.Y., White, D.J., Hartenstein, V., Eliceiri, K., Tomancak, P. and
905   Cardona, A. (2012) Fiji: an open-source platform for biological-image analysis. *Nat Methods*, **9**,
906   676-682.
907   Schott, S., Ambrosini, A., Barbaste, A., Benassayag, C., Gracia, M., Proag, A., Rayer, M., Monier, B. and
908   Suzanne, M. (2017) A fluorescent toolkit for spatiotemporal tracking of apoptotic cells in living
909   Drosophila tissues. *Development.*, **144**, 3840-3846. doi: 3810.1242/dev.149807. Epub 142017 Sep
910   149804.
911   Shao, E., Lin, L., Liu, S., Zhang, J., Chen, X., Sha, L., Huang, Z., Huang, B. and Guan, X. (2018) Analysis of
912   Homologs of Cry-toxin Receptor-Related Proteins in the Midgut of a Non-Bt Target, Nilaparvata
913   lugens (Stal) (Hemiptera: Delphacidae). *J Insect Sci*, **5**.
914   Shao, E., Liu, S., Lin, L. and Guan, X. (2013) Proteolytic processing of Bacillus thuringiensis toxin Cry1Ab in
915   rice brown planthopper, Nilaparvata lugens (Stål). *J Invertebr Pathol*, **114**, 255-257.
916   Shaw, R.L., Kohlmaier, A., Polesello, C., Veelken, C., Edgar, B.A. and Tapon, N. (2010) The Hippo pathway
917   regulates intestinal stem cell proliferation during Drosophila adult midgut regeneration.
918   *Development*, **137**, 4147-4158. doi: 4110.1242/dev.052506. Epub 052010 Nov 052510.
919   Shaya, O., Binshtok, U., Hersch, M., Rivkin, D., Weinreb, S., Amir-Zilberstein, L., Khamaisi, B., Oppenheim,
920   O., Desai, R.A., Goodyear, R.J., Richardson, G.P., Chen, C.S. and Sprinzak, D. (2017) Cell-Cell
921   Contact Area Affects Notch Signaling and Notch-Dependent Patterning. *Dev Cell*, **40**, 505-
922   511.e506.
923   Soberon, M., Gill, S.S. and Bravo, A. (2009) Signaling versus punching hole: How do Bacillus thuringiensis
924   toxins kill insect midgut cells? *Cell Mol Life Sci*, **66**, 1337-1349.
925   Stevens, T., Song, S., Bruning, J.B., Choo, A. and Baxter, S.W. (2017) Expressing a moth abcc2 gene in
926   transgenic Drosophila causes susceptibility to Bt Cry1Ac without requiring a cadherin-like protein
927   receptor. *Insect Biochem Mol Biol*, **80:61-70.**, 10.1016/j.ibmb.2016.1011.1008. Epub 2016 Nov
928   1030.
929   Tian, A. and Jiang, J. (2014) Intestinal epithelium-derived BMP controls stem cell self-renewal in
930   Drosophila adult midgut. *Elife*, **3:e01857.**, 10.7554/eLife.01857.

931 Toret, C.P., D'Ambrosio, M.V., Vale, R.D., Simon, M.A. and Nelson, W.J. (2014) A genome-wide screen
932   identifies conserved protein hubs required for cadherin-mediated cell-cell adhesion. *J Cell Biol*,
933   **204**, 265-279.
934 Vachon, V., Laprade, R. and Schwartz, J.L. (2012) Current models of the mode of action of Bacillus
935   thuringiensis insecticidal crystal proteins: a critical review. *J Invertebr Pathol*, **111**, 1-12.
936 Vriz, S., Reiter, S. and Galliot, B. (2014) Cell death: a program to regenerate. *Curr Top Dev Biol*, **108**, 121-
937   151.
938 Watnick, P.I. and Jugder, B.E. (2019) Microbial Control of Intestinal Homeostasis via Enteroendocrine Cell
939   Innate Immune Signaling. *Trends Microbiol*, **4**, 30240-30249.
940 Zeng, X., Chauhan, C. and Hou, S.X. (2010) Characterization of midgut stem cell- and enteroblast-specific
941   Gal4 lines in drosophila. *Genesis*, **48**, 607-611. doi: 610.1002/dvg.20661.
942 Zeng, X. and Hou, S.X. (2015) Enteroendocrine cells are generated from stem cells through a distinct
943   progenitor in the adult Drosophila posterior midgut. *Development.*, **142**, 644-653. doi:
944   610.1242/dev.113357.
945 Zhai, Z., Boquete, J.P. and Lemaitre, B. (2017) A genetic framework controlling the differentiation of
946   intestinal stem cells during regeneration in Drosophila. *PLoS Genet.*, **13**, e1006854. doi:
947   1006810.1001371/journal.pgen.1006854. eCollection 1002017 Jun.
948 Zwick, R.K., Ohlstein, B. and Klein, O.D. (2019) Intestinal renewal across the animal kingdom: comparing
949   stem cell activity in mouse and Drosophila. *Am J Physiol Gastrointest Liver Physiol.*, **316**, G313-
950   G322. doi: 310.1152/ajpgi.00353.02018. Epub 02018 Dec 00313.

951

952

Figure legends

Figure 1: Crystals of *Btk* Cry protoxins induce EC death and stimulate proliferation of intestinal stem cells

(**A-D**) Flies were fed with water (blue, control-ctrl), $Btk^{\Delta Cry}$ spores (green), Btk^{SA11} spores (purple) or Crystals (pink). The initial dose provided with the food to flies was 10^6 CFU fly/4 cm² (this dose is used in all the following experiments presented in this article).

(**A**) Left panel: Quantification of dead ECs 24h post ingestion (PI) in the posterior midgut (R4 region). EC apoptosis was monitored by expressing the Caspase 3 sensor (Casp:: GFP) using the *myo1A-GAL4* EC driver *(myo1A>Casp::GFP)*. With this transgenic combination, the GFP is detectable only when the Caspase 3 is activated in ECs. Right panel: *myo1>GFP* midguts labeled with the anti-cleaved Caspase 3 antibody (red).

(**B**) Quantification of mitoses using the anti-PH3 antibody in the whole midgut 24h PI.

(**C**) ISC Number in the R4 region of *esg>GFP* flies 24, 72, and 120h PI.

(**D**) EC number in the R4 region of *myo1A>GFP* flies 24, 72, and 120h PI.

n=number of midguts; ns=not significant; * ($P \leq 0.05$); ** ($P \leq 0.01$), *** ($P \leq 0.001$).

Figure 2: Btk^{SA11} spores induce an increase in EB, EEP and EEC numbers

(**A-D**) Flies were fed with water, $Btk^{\Delta Cry}$ spores, Btk^{SA11} spores or Crystals.

(**E-E''**) Flies were fed with Btk^{SA11} spores.

(**A-C**) Control (water-ctrl): blue bars; $Btk^{\Delta Cry}$ spores: green bars; Btk^{SA11} spores: purple bars; Crystals: pink bars.

(**A**) Number of EBs in the R4 region of *Su(H)>CD8::GFP* flies 24, 48, and 72h PI.

(**B** and **C**) Number of EEPs (B) and EECs (C) in the R4 region of *esg>GFP* flies 24, 48, and 72h PI.

(**D-E''**) R4 region of *esg>GFP* flies labeled with anti-Pros (Red). GFP was expressed in ISCs, EBs and EEPs, and Pros was expressed in EEPs (yellow arrows in D) and EECs (red arrows in D).

(E-E'') PH3 staining (blue) marks mitosis. Pink arrows point to dividing EEPs and blue arrows point to dividing ISCs.

n=number of samples; * ($P \leq 0.05$); ** ($P \leq 0.01$), *** ($P \leq 0.001$).

Figure 3: EEC excess arises from newborn EEPs after ingestion of Btk^{SA11} crystals

(**A**) Schema of the experimental design for the *esg-ReDDM* cell lineage used in this entire figure.

(**B-E''**) R4 region of *esg-ReDDM* flies. Midguts were stained for Pros (blue) and DAPI which marks nuclei (white in B, C, D and E). (B-E'') show the different cell types which either existed before the ingestion (green and red) or arise after the ingestion (red only) of water (B-B'', Ctrl), $Btk^{\Delta Cry}$ spores (C-C'') or Btk^{SA11} spores (D-D'') and Crystals (E-E''). ISCs were GFP+ RFP+ DAPI+ with small nuclei; EBs were GFP+ RFP+ DAPI+ with bigger nuclei; EEPs were GFP+ RFP+ Pros+ DAPI+; new EECs were RFP+, Pros+ DAPI+; old EECs were Pros+ DAPI+; new ECs were RFP+ DAPI+ with polyploid big nuclei and old ECs were DAPI+ with very big nuclei.

(**F**) Counting old EECs (Pros+ RFP-) and new EECs (Pros+ RFP+) in the conditions described in (B-E)

(**G**) Counting old ECs (DAPI+) and new ECs (DAPI+ RFP+) in the conditions described in (B-E)

n=number of samples; ns=not significant; * ($P \leq 0.05$); *** ($P \leq 0.001$).

Figure 4: Btk bioinsecticide decreases ISC-Progenitor cell-cell adhesion

(**A-I**) *esg>UAS-GFP* or) *esg>UAS-GFP, Tomato::shg* (B, D, F and H) *Drosophila* midgut R4 region 24h PI of water (A-B Ctrl), $Btk^{\Delta Cry}$ spores (C-D), Btk^{SA11} spores (E-F) or crystals (G-H).

(**A, C, E,** and **G**) Midguts are labeled with anti-Armadillo (Arm) (red in A, C, E, and G) which strongly marks the adherent junctions between ISC and progenitors (green) and Dapi (blue).

(**A', C', E',** and **G'**) correspond to the single Arm channel.

(**B, D, F** and **H**) Midguts are labelled for Pros (blue), DE-Cadherin (red) and ISCs and progenitors (green).

Red arrows point to the high intensity of adherens junctions staining between ISC and progenitors. Yellow arrows point to the weak intensity of adherens junction staining. Note that the high intensity of adherens junction staining is associated with ISC/EB interaction while the weak intensity of adherens junction staining is associated with ISC/EEP interaction (blue stars mark EEPs in B, D, F and H)

(**I**) Graph representing the percentage of the different categories of cell contact intensity between ISCs and progenitors in the experimental conditions shown in (A, C, E, and G). 15<n<18 intestines. Weak = Contact Intensity/Membrane Intensity<1.3; Mild = 1.3<Contact Intensity/Membrane Intensity<1.6; Strong = Contact Intensity/Membrane Intensity>1.6.

Figure 5: Increasing adherens junction strength rescues crystal-dependent cell fate diversion

(**A-F**) *esg-ReDDM>DE-Cad Drosophila* midgut R4 region. These flies specifically overexpress the DE-Cad in ISCs and progenitors. Flies were fed with water (A-A', and blue in E, Ctrl), $Btk^{\Delta Cry}$ spores (B, B', and green in E), Btk^{SA11} spores (C, C' and purple in E) or Crystal (D-D' and pink in E) and observed 72h PI (see Figure 3A for the experimental design). In (A-D') blue arrows point to old EECs and red arrows newborn ECs. (E) Number of old EECs (Pros+ RFP-) and new EECs (Pros+ RFP+) in the conditions described in (A-D).

 (**F**) Graph representing the percentage of the different categories of cell contact intensity between ISCs and progenitors in the experimental conditions shown in (Figure S4 A-D'). Weak = Contact Intensity/Membrane Intensity<1.3; Mild = 1.3<Contact Intensity/Membrane Intensity<1.6; Strong = Contact Intensity/Membrane Intensity>1.6.

(**G-G''**) Cell aggregation assays on S2 cells expressing the DE-Cadherin::GFP. Cells placed under constant rotation were incubated with or without *Bt* crystals or purified Cry protoxins (Cry1Ab or Cry1Ac) for 1h (G), 2h (G') or 3h (G''). Each scatter plot represents the area (µm2) of all objects (aggregates or individual cells) obtained from 3 independent experiments. Representative images of cell aggregates formed in aggregation assays are shown in supplemental data (Figure S4E).

n=number of samples, ns (non-significant), * ($P \leq 0.05$), ** ($P \leq 0.01$), *** ($P \leq 0.001$).

Figure 6: Cry1A toxins mimic *Btk* crystal effects

(**A-C**) *esg>GFP* flies fed with water (blue bars, Ctrl), Btk^{Cry1Ac} spores (fuchsia bars in A), Cry1Ac crystals (pink bars in A), Btk^{Cry1Ab} spores (fuchsia bars in B), Cry1Ac protoxins (light pink bar in C), Cry1Ac activated toxins (pink bars in C), Cry2Aa protoxins (light beige bar in C) and Cry2Aa activated toxins (beige bar in C).

(**A** and **B**) Number of EEPs or EECs in the R4 region 72h PI

(**C**) Number of Pros+ cells in the R4 region 72h PI

(**D** and **E**) Western Blot from dissected intestines using a polyclonal Anti-Cry1A antibody detecting both the protoxins and the activated forms of Cry1A family of toxins.

(**D**) (left lane) 0h corresponds to Btk^{SA11} spores extemporaneously resuspended in water. (Right part of the blot) Btk^{SA11} spores from incubated *ex vivo* (control) in water at 25°C for the period of the experiment. We mainly detect the protoxin forms of Cry1A at 130kDa (arrowhead). (Left part of the blot) Proteins extract from midgut of flies fed by the same Btk^{SA11} preparation (T 0h) at 4h

32

1042   and 1, 3 and 6 days PI. The 130kDa protoxins are still visible. The 67kDa activated form appears

1043   as early as 4h (arrow). 6 days PI no more toxins are detected in the midgut.

1044   (**E**) Flies fed 2 days with water (Ctrl, left part) or with purified crystals (right part). Protoxins

1045   (130kDa) are present in the membrane fraction (Mb) in both the anterior (ant) and the posterior

1046   (post) midgut. The 67kDa activated forms are present in the membrane fraction of both the anterior

1047   and posterior midgut and in the cytoplasmic fraction (Cyto) of the posterior midgut.

1048   n=number of samples. *** (P ≤ 0.001).

1049   **Figure 7: Cry1A toxins interfere with progenitor fate behavior**

1050   **Notch ON:** in *Drosophila*, 90% of ISC daughter cells commit to the EB/EC fate owing to the

1051   strong activation of the Notch signaling pathway in the EBs. The adherens junction DE-Cadherin

1052   (DE-Cad)-dependent are required to permit the interaction between the Delta ligand in ISC and

1053   the Notch receptor in EB.

1054   **Notch OFF:** Ingestion of Cry1A toxins impedes the DE-Cad homophilic interaction between the

1055   ISCs and their progenitor daughter cells, reducing the activation of Notch signaling in progenitors.

1056   Consequently, progenitors adopt an EEP/EEC fate.
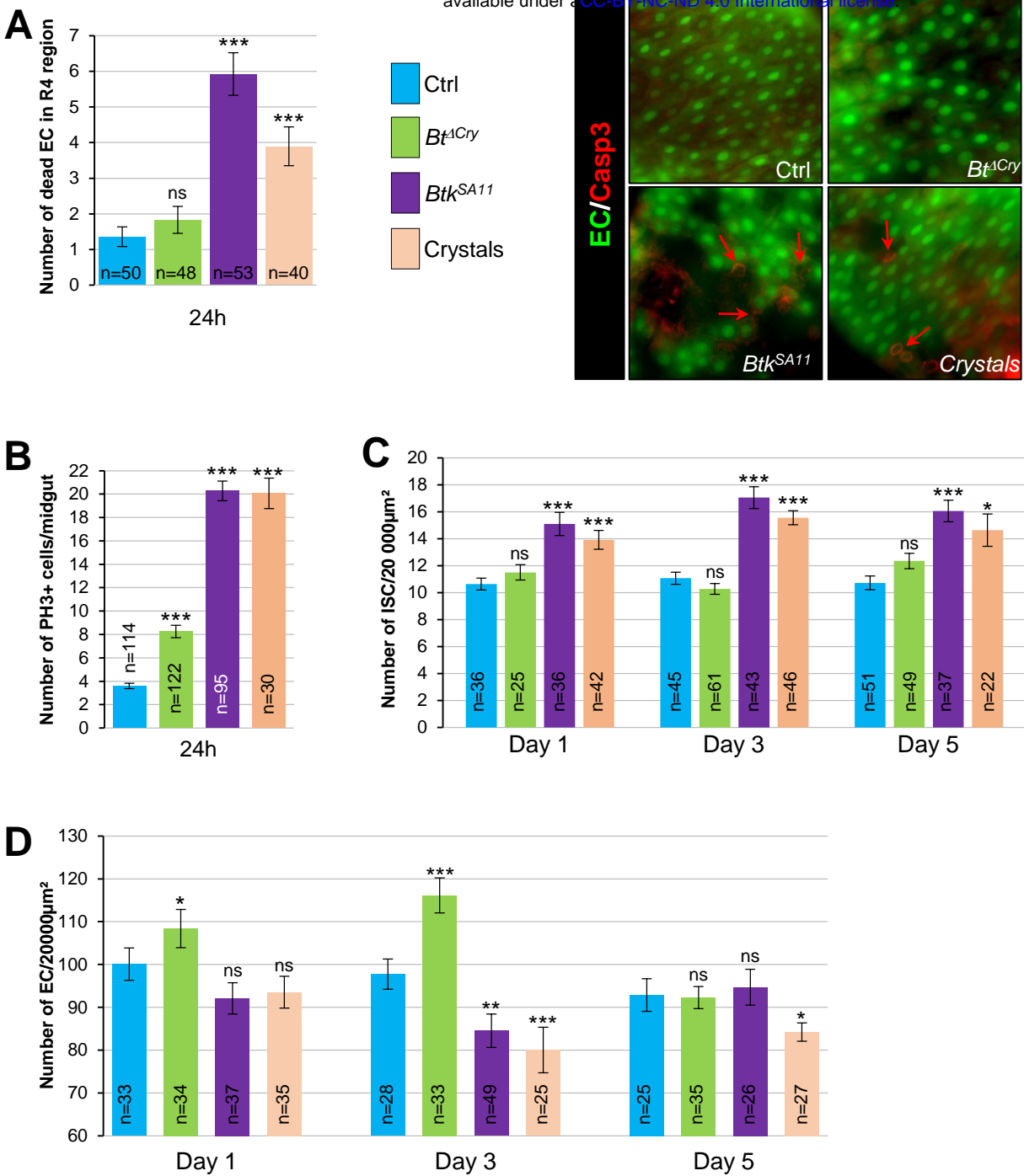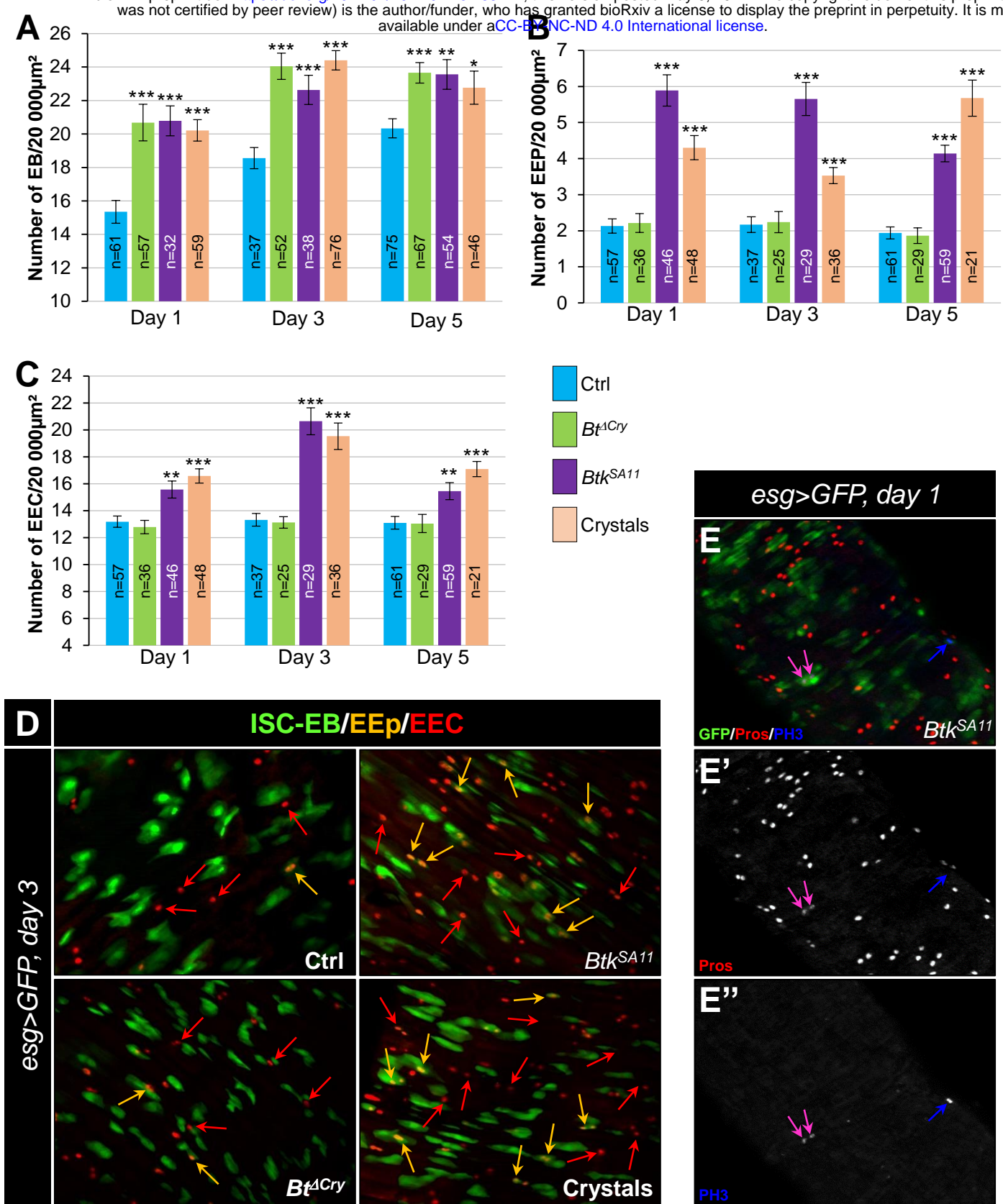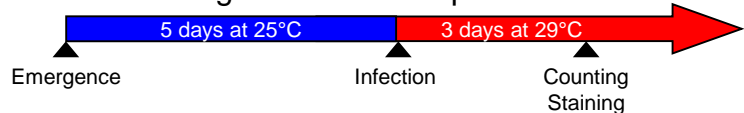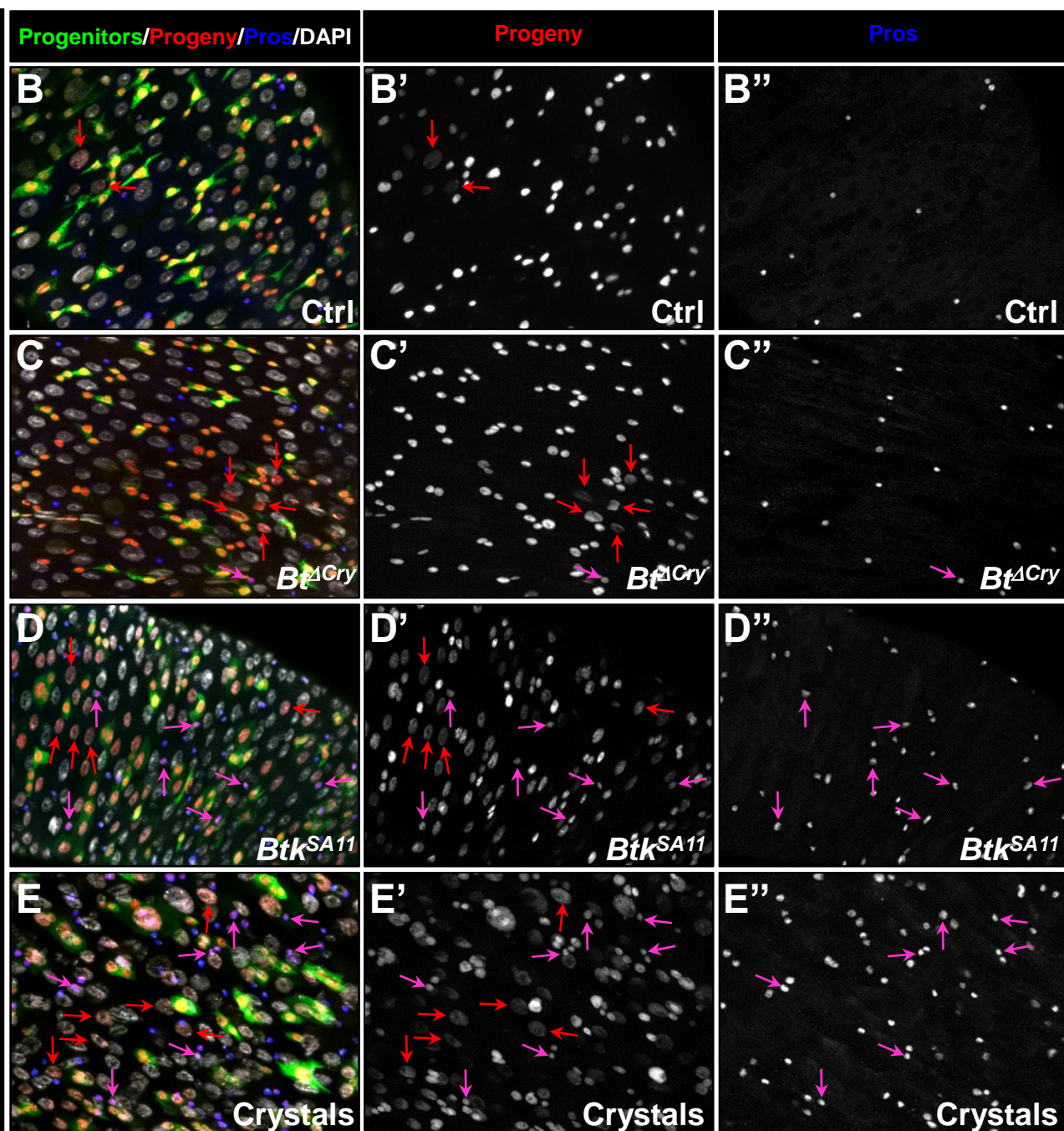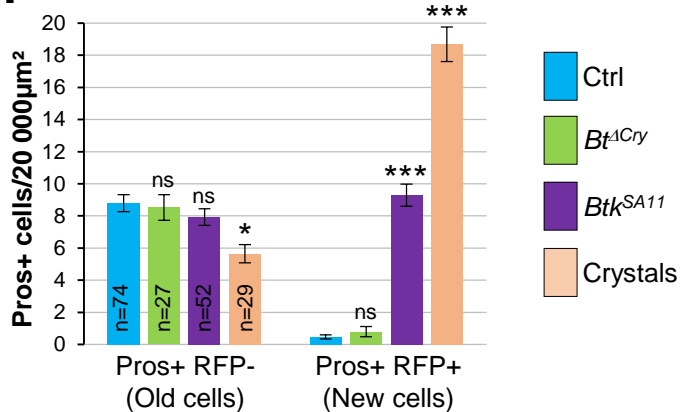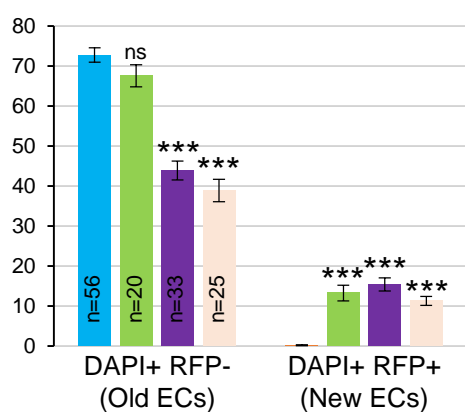
33
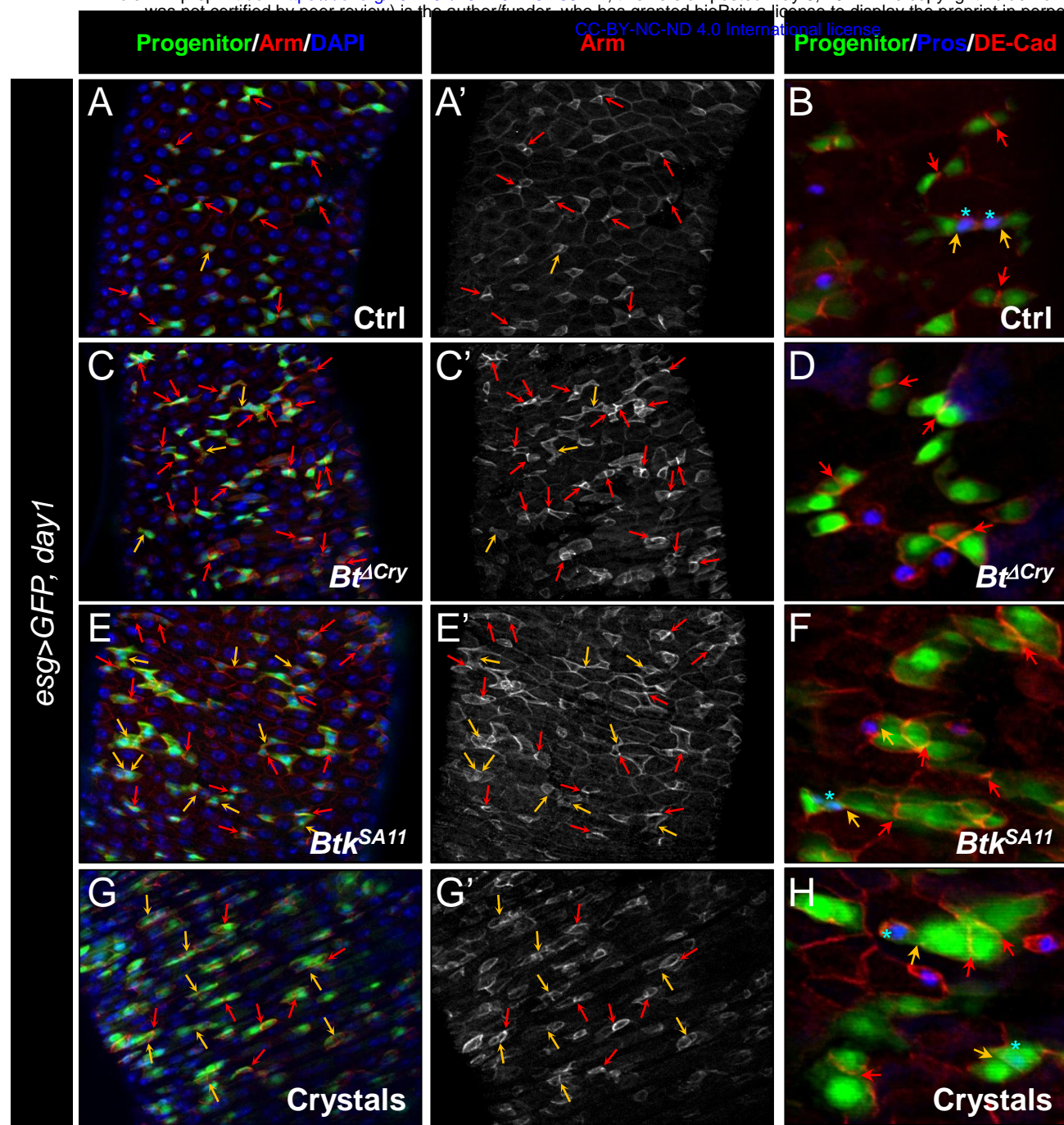
Figure 1

Figure 2
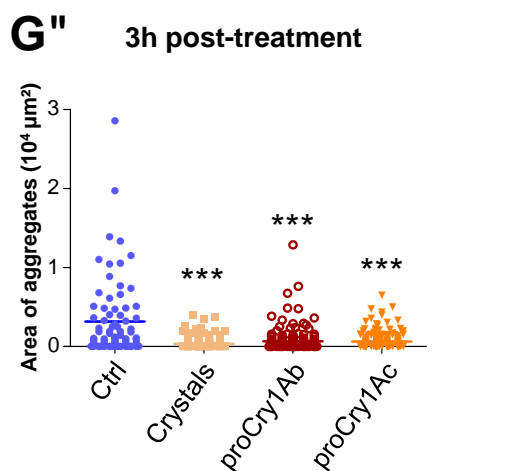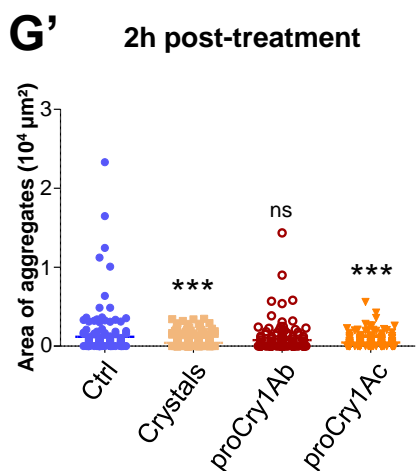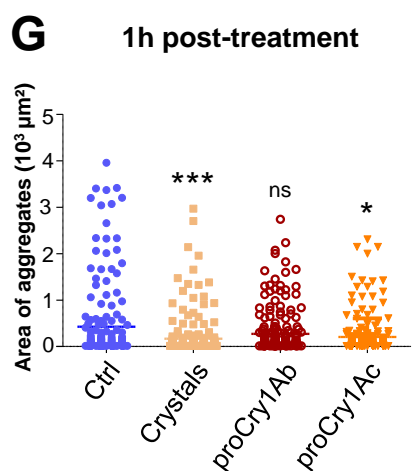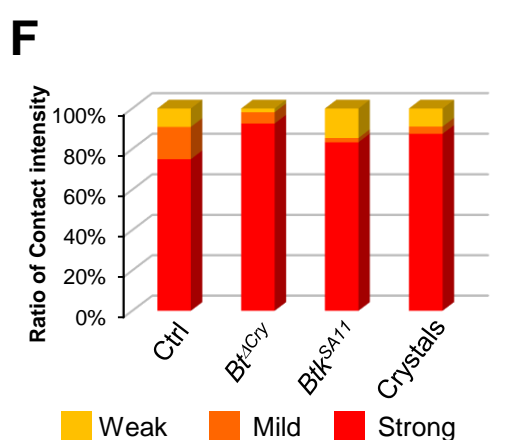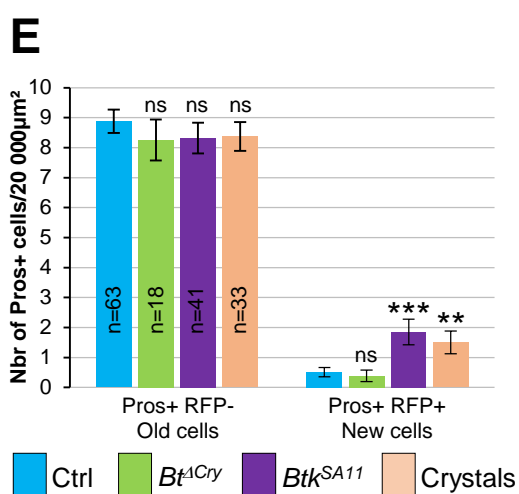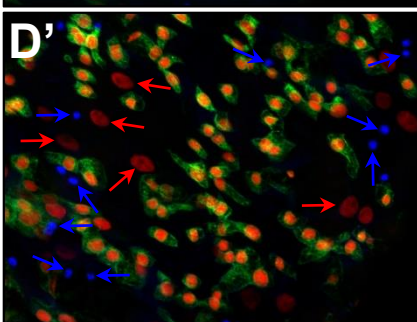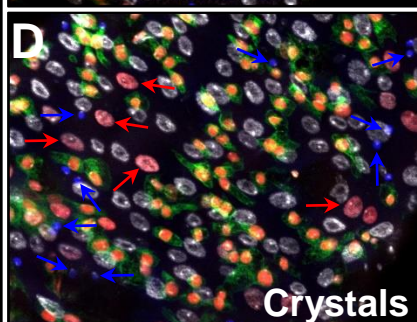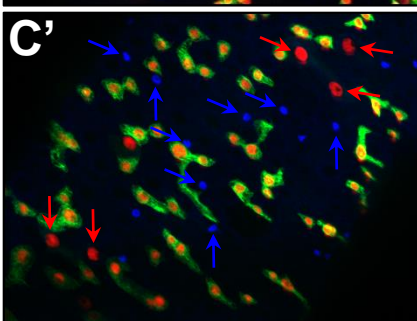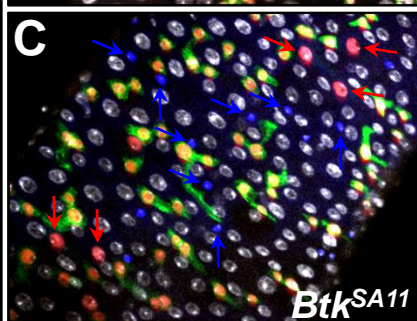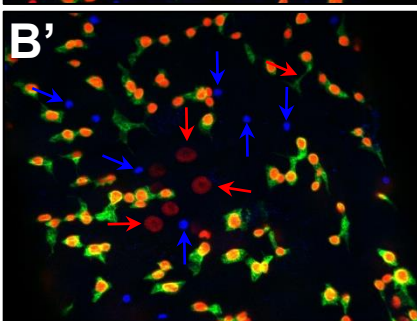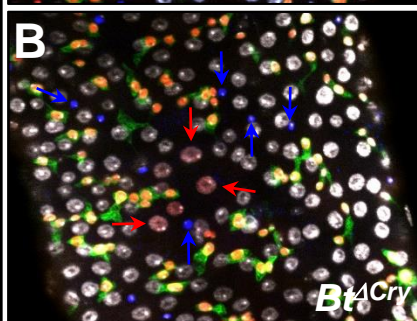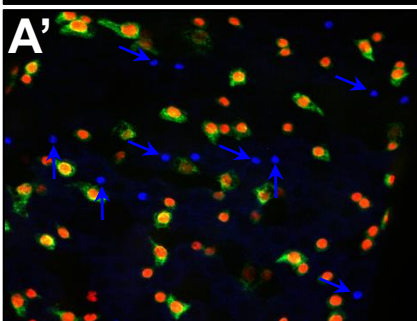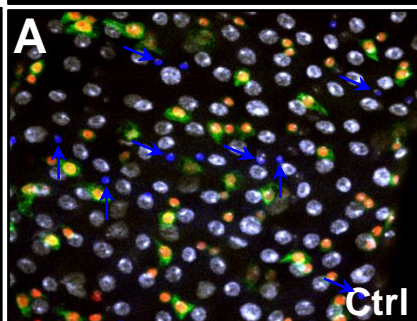
Figure 3

Figure 4

Figure 5

Figure 6

Figure 7